In-vivo Transcriptomic Profiling of Systemic Aging using Cell Encapsulation

Omid Mashinchian[1,2,*], Xiaotong Hong[1,3,*], Eugenia Migliavacca[1], Christophe Boss[1], Filippo De Franceschi[1], Joris Michaud[1], Emmeran Le Moal[4], Jasmin Collerette-Tremblay[4], Joan Isern[3], Sylviane Metairon[1], Frederic Raymond[1], Patrick Descombes[1], Nicolas Bouche[1], Pura Muñoz-Cánoves[3,5], Jerome N. Feige[1,2,#], C. Florian Bentzinger[1,4,#]

1. Nestle Research
   EPFL Innovation Park, Building H
   Lausanne, Switzerland
2. School of Life Sciences
   École Polytechnique Fédérale de Lausanne (EPFL)
   Lausanne, Switzerland
3. Centro Nacional de Investigaciones Cardiovasculares (CNIC), Madrid, Spain
4. Département de Pharmacologie-Physiologie
   Institut de Pharmacologie de Sherbrooke
   Centre de Recherche du Centre Hospitalier Universitaire de Sherbrooke
   Faculté de Médecine et des Sciences de la Santé
   Université de Sherbrooke
   Sherbrooke, Canada
5. Department of Experimental and Health Sciences, Pompeu Fabra University (UPF), CIBER on Neurodegenerative Diseases (CIBERNED) and Institució Catalana de Recerca i Estudis Avançats (ICREA), Barcelona, Spain

* Equal contribution

\# Corresponding authors & equal contribution:
Florian Bentzinger: *cf.bentzinger@usherbrooke.ca*
Jerome Feige: *Jerome.Feige@rd.nestle.com*

Abstract

Sustained exposure to a young systemic environment rejuvenates aged organisms and promotes cellular function. However, due to the intrinsic complexity of tissues it remains challenging to pinpoint niche-independent effects of circulating factors on specific cell populations. Here we describe a method for the encapsulation of human and mouse skeletal muscle progenitors in diffusible polyethersulfone hollow fiber capsules that can be used to profile systemic aging *in-vivo* independent of heterogeneous short-range tissue interactions. We observe that circulating long-range signaling factors in the old systemic environment have dominant effects on inflammation related processes that act in concert with increased activity of Myc and E2F transcription factors. Importantly, this signature is conserved across species and a subset of processes altered in encapsulated progenitors, are also affected in brain tissue of heterochronic parabionts. Altogether, our study characterizes the cellular signature of systemic aging mediated by direct effects of long-range signaling factors and identifies conserved therapeutic targets for systemic rejuvenation.

Main

Systemic crosstalk between tissues has emerged as an important determinant of organismal aging[1]. Supporting this notion, several features of tissue aging can be slowed or reversed by heterochronic parabiosis[2, 3]. Restoration of a youthful systemic environment has been shown to improve the function of muscle, heart, liver, brain and other tissues in aged mice[4-11]. Interestingly, the positive effects of young blood on aged tissues appear to be milder than the pronounced negative effects of aged blood on young tissues[12]. This observation suggests the presence of dominant pro-aging factors in the systemic circulation, which cross-talk with local tissue niches to induce the global decline in organ function associated with old age. Recent studies have aimed at identifying the circulating factors involved in systemic aging, and some of the experimental interpretations have led to considerable controversy in the field[13].

It has long been known that a range of endocrine hormones are perturbed in later stages of life. Aging affects the somatotroph axis leading to decreased levels of growth hormone and IGF-1[14]. Levels of sex hormones such as testosterone and estrogen drop in aged individuals[15]. Old age is also associated with increased systemic inflammation that often goes along with a metabolic syndrome attributed to insulin resistance and an excessive flux of fatty acids[16, 17]. Next to these broad biological processes, several distinct pro- and anti-aging factors have been identified in the systemic environment. These include GDF15, eotaxin, β2-microglobulin, and transforming growth factor-β, which negatively affect brain or muscle tissue in aging[8, 10, 18-20]. Factors activating Notch, GDF11 and TIMP2, on the other hand, have been suggested to have rejuvenating effects[4, 21-23].

The modulation of age affected signaling pathways, represents a promising alternative to supplying or inhibiting systemic factors for rejuvenation. However, the study of pathways that are responsive to systemic changes is complicated by the heterogeneous composition of tissues, which contain a multitude of cell types that communicate through secreted short-range signals. Systemic factors do not always act in a direct manner on tissue resident cell populations but can instead trigger paracrine propagation and modulation of signals through accessory cell types in the niche. In the intestinal crypt, paneth cells are known to transmit systemic signals induced by caloric restriction to intestinal stem cells[24]. Moreover, fibro-adipogenic progenitors, an age-affected support cell population for skeletal muscle stem cells, are highly susceptible to systemic cytokines[25, 26]. Factors in the aging circulation also

alter accessory cell signaling in the neurogenic niche, which contributes to neural stem cell dysfunction[27]. These examples illustrate that profiling of aging pathways that are directly affected by systemic long-range signaling factors, requires an approach that allows to subtract the pervasive noise generated by the heterogeneous tissue environment.

Here we present a method that allows for the encapsulation of homogeneous cell populations in diffusible hollow fiber capsules that can be transplanted subcutaneously to profile the effects of an aged systemic environment in the absence of short-range cellular interactions (**Fig. 1a**). This approach makes it possible to expose cells from multiple species and different genetic backgrounds to heterotypic physiological environments to characterize gene-environment relationships. It provides a paradigm to disentangle direct effects mediated by systemic signals from cell intrinsic programming and input relayed by accessory cells in the tissue niche.

Encapsulation of myogenic progenitors in PES hollow fiber membranes

Given their wide use in ultra-filtration applications, their oxidative, thermal and hydrolytic stability, and their favorable mechanical properties we chose polyethersulfone (PES) hollow fiber membrane (HFM) tubes for encapsulation of primary human (hskMPs) and C57BL/6J mouse derived skeletal muscle progenitors (mskMPs)[28]. Importantly, PES fibers are biocompatible, have low immunogenicity, and become vascularized when subcutaneously implanted[29]. In order to maximize the number of encapsulated cells and, at the same time, allow for adequate oxygen diffusion throughout the capsule, we selected a tubular HFM with an outer diameter of 0.9 mm and an inner diameter of 0.7 mm (**Fig. 1b**). The spongy-like, cross-linked architecture of PES-HFM allows for the diffusion of molecules up to 280 kDa freely through the membrane but prevents infiltration by cells. To provide a suitable adhesion matrix, cells were embedded in growth factor reduced Matrigel[30]. Based on flow cytometric quantification of apoptosis, Matrigel resulted in cellular viability >90% following a ten-day culture period that was superior to other extracellular matrix substrates or hydrogel (**Supplementary Fig. 1a-c**). After mounting of the HFM to an adaptor hub, the exposed end and the external hub interface were sealed using a bio-compatible photopolymerizing medical grade polyacrylate adhesive (**Fig. 1c and Supplementary Fig. 1d**). Sealing of devices was verified using a submersion air pressure decay test. Trypsinized

hskMPs or mskMPs mixed with Matrigel were injected into the capsule trough the adaptor hub and the loaded capsule was transferred onto a 3D printed autoclavable USP Class VI plastic cutting and sealing platform (**Supplementary Fig. 1e,f**). Following cutting of the adaptor hub, the loaded capsule remained protected in the UV impermeable plastic device while the second adhesive seal was photopolymerized.

In-vitro characterization of encapsulated myogenic progenitors

For validation of our experimental setup and to interrogate the behavior of encapsulated cells, we performed a series of *in-vitro* experiments. Capsules loaded with hskMPs or mskMPs were placed into culture dishes, immersed in growth media, and were maintained on a horizontal shaker platform in a tissue culture incubator. Terminal deoxynucleotidyl transferase dUTP nick end labeling (TUNEL) staining of cryosections from capsules that were kept in culture for ten days revealed that over 90% of the cells remained viable (**Fig. 2a,b**)**.** Demonstrating proper oxygen and nutrient supply, cell density increased slightly in capsules in culture (**Fig. 2c,d**). Following ten days in culture, hskMPs and mskMPs were distributed across the entire diameter of the capsules (**Fig. 2e,f**). Over the ten-day encapsulation time-course, hskMPs and mskMPs showed a mild ≤37% reduction in the number of cells positive for the myogenic marker Pax7, while ≥80% of the cells remained positive for MyoD (**Fig. 2g-l**). Indicating that the capsule 3D context favors the maintenance of myogenic markers, hskMPs in classic 2D culture downregulated Pax7 and MyoD expression by 62% and MyoD by 37% over the same ten-day period (**Supplementary Fig. 1g**). After ten days of encapsulation, proliferative cells could be recovered from the capsules by enzymatic liberation (**Supplementary Fig. 1h**). Growth factor deprivation over a four-day differentiation period, induced a robust ≥80% reduction of Pax7 in hskMPs and mskMPs, reduced MyoD by 43% in human cells, and, in spite of spatial restraints due to 3D embedding, increased the terminal differentiation marker myosin heavy chain (MHC) by ≥170% in both cell types (**Fig. 2m-s**)**.** Collectively, these observations demonstrate that encapsulated hskMPs and mskMPs remain viable and proliferative, retain the expression of myogenic markers, and are capable to respond to pro-differentiative signals.

In-vivo characterization of encapsulated myogenic progenitors

We next established the capsule implantation and recovery procedure in adult male C57BL/6J mice. The animals were anesthetized, and incisions were made on the back slightly posterior to each scapula. Three to four capsules containing hskMPs or mskMPs were introduced in varying locations into the subcutaneous fascia over the ribcage separated by 3-5 mm (**Fig. 3a**). Capsule insertion was performed using a hypodermal plastic tube with a sliding metal plunger. In case of hskMPs, an immune reaction to secreted xenogeneic proteins was prevented by subcutaneous implantation of an osmotic pump supplying the immunosuppressant FK-506 on the contralateral flank. Out of a panel of 40 inflammatory markers, not a single factor was upregulated in serum from C57BL/6J mice that received capsules containing syngeneic cells in the absence of immunosuppression (**Supplementary Fig. 2a and Supplementary Table 1**). After ten days *in-vivo* the capsules showed vascularization and minimal connective tissue build-up (**Fig. 3b**). TUNEL apoptosis assays using cross-sections from explanted capsules revealed that ≥80% of hskMPs and mskMPs remained viable (**Fig. 3c,d**), and that Pax7, MyoD and MHC were still expressed by the cells (**Fig. 3e-m**).

In-vivo profiling of systemic aging

To apply our systemic profiling protocol, we implanted young and aged C57BL/6J mice for ten days with capsules containing hskMPs and mskMPs. RNA was sufficient for genome wide transcriptomic profiling for both cell types (**Supplementary Fig. 3a,b**). Gene set enrichment analysis using the hallmark database revealed that targets of the Myc and E2F family of transcription factors that have previously been implicated in aging and senescence, were induced in both hskMPs and mskMPs exposed to an aged systemic environment[31-33] (**Fig. 4a-c and Supplementary Table 2,3**). Myc is induced by mitogens and inflammatory processes[34, 35]. However, aging is known to downregulate systemic sex hormones and the somatotroph axis leading to decreased levels of critical growth factors such as IGF-1 and growth hormone[14]. Thus, in order to determine whether Myc induction is due to elevated systemic proinflammatory markers, we profiled serum from aged C57BL/6J mice and detected increased levels of BLC (CXCL13), ICAM-1 (CD54), Leptin, MIG (CXCL9) and TIMP-1 when compared to the young condition (**Supplementary Fig. 4a and**

Supplementary Table 4). Further gene set analysis revealed that the categories myogenesis, epithelial–mesenchymal transition (EMT), interleukin, interferon, and p53 signaling were found to be suppressed in hskMPs and mskMPs by an aged systemic environment (**Fig. 4d and Supplementary Table 5,6**). To determine which features of aging are directly controlled by long-range secreted factors in the systemic circulation as opposed to signals transduced by the physiological tissue niche, we compared our dataset to freshly isolated myogenic progenitors from young and aged C57BL/6J mice (**Fig. 4e and Supplementary Table 7,8**). Next to many exclusively niche controlled processes, we observed an overlap with respect to an upregulation of Myc and E2F targets, as well as a downregulation of myogenesis and EMT. Collectively, these results demonstrate an involvement of processes related to inflammation that act in concert with increased Myc and E2F transcription factors in systemically imposed cellular aging.

Systemically induced aging signatures are conserved across tissues

Finally, we set out to test whether processes affected by an aged systemic environment in encapsulated hskMPs and mskMPs are also changed in tissues of mice undergoing heterochronic parabiosis. To this end, we compared gene ontology (GO) terms enriched in transcriptional profiling of brain tissue obtained from heterochronic relative to isochronic parabionts to our study[36]. This analysis revealed that GO terms for basic cellular processes such as RNA processing are upregulated by an aged systemic environment in both datasets, while interferon and innate immune responses are suppressed (**Supplementary Table 9,10**). Thus, the transcriptional response to a differentially aged systemic environment is partially conserved across species and cell types.

Discussion

Our study demonstrates that encapsulation of syn- and xenogeneic cells allows for systemic transcriptional profiling independent of short-range heterogenous cellular interactions. Compared to other types of capsules that have been used in mice, for instance planar macroencapsulation devices[37], hollow fiber capsules are miniaturized to a diameter of 0.7 mm and a length of 1cm that can be varied according to need. PES is one of the most frequently used polymers in medical applications and, due to its low immunogenicity, has been studied extensively in the context of artificial organs and medical devices used for blood purification in humans[38-41]. Underlining its biocompatibility, we observed that subcutaneous implantation of PES capsules does not induce systemic inflammatory markers. Given, the broad interest of the aging field in using skeletal muscle stem cells as a model system for tissue maintenance and repair[42-44], we selected myogenic progenitors for our profiling experiments. For implantation, we chose the myofascia of the ribcage that is easily accessible and that is in contact with the extensive subcutaneous vasculature, skeletal muscle, and bone, resembling the systemic environment myogenic progenitors are exposed to *in-situ*. We observed that after explantation of capsules viable proliferative cells can be enzymatically liberated. Thus, our method is not limited to bulk transcriptomic profiling, but can be modified to allow for single cell sequencing or for the *in-vitro* study of long-lasting intrinsic adaptations induced by exposure to an aged systemic environment.

Worldwide, the population of aged individuals has grown to an unprecedented size, and by 2050 more than 430 million people will be over the age of 80[44]. The characterization of bona fide aging signatures in defined cell populations independent of the heterogenous niche context, will allow for the identification of novel therapeutic targets for the systemic treatment of age-associated cellular dysfunction in frail individuals. Importantly, cell encapsulation allows to filter out the dominant noise of the aged tissue that is in direct contact with the cell population of interest. Only long-range signaling factors are able to diffuse over the capsule membrane, which allows to read out effects of these molecules independent of extracellular matrix, heterologous cell-cell contacts, and short-range paracrine growth factors secreted by accessory cells in the tissue. Therefore, in contrast to profiling of cells directly extracted from aged niches or following parabiotic pairing, encapsulation allows to obtain a pure and unbiased transcriptional signature of the systemic environment in defined cell types

of choice and makes this amenable to cellular signaling across different species. As such, encapsulation is not an alternative to studying cells in their endogenous niche, but a complementary approach that allows to dissect specific questions on systemic versus tissue-mediated interactions.

Using gene set enrichment analysis, we observed that activity of the Myc and E2F family of transcription factors is strongly induced by systemic aging in both mouse and human myogenic progenitors. E2F1, which interacts with the retinoblastoma tumor suppressor, has been shown to be a key mediator of cellular senescence[33]. Mice haploinsufficient for Myc exhibit an increased lifespan and are resistant to osteoporosis, cardiac fibrosis and immunosenescence[31]. Rapalogs, which inhibit the activity of mammalian target of rapamycin complex 1, increase life span and delay hallmarks of aging in many species. It has been shown that the rapalog RAD001, counter-regulates Myc in aged kidneys[32]. Moreover, Myc is known to be induced by mitogens and inflammatory processes[34, 35]. In agreement with these observations, we detected significantly increased levels of systemic pro-inflammatory factors in aged mice. Interestingly, fundamental biological mechanisms such as RNA processing and inflammation related processes affected in our encapsulation study, were also changed in brain tissue of heterochronic parabionts. These observations fall well in line with age associated defects at multiple levels of the immune system, including decreased B and T cell production and altered lymphocyte function that are commonly termed "inflammaging"[45, 46]. Altogether, our study identifies these cellular mechanisms as a direct consequence of systemic aging that occur independent of the influence of heterologous tissue-resident accessory cells. In contrast, comparison to myogenic cells directly isolated from skeletal muscle tissue, revealed that processes such as fatty acid metabolism, G2M checkpoint determination, and oxidative phosphorylation are imposed by the aged niche and are not directly affected by the systemic environment.

Importantly, our protocol is not limited to aging and will also allow to assess the impact of other multisystemic conditions on defined cell populations of interest. Moreover, in future applications, the combination of encapsulation technology with genetically engineered or induced pluripotent stem cell (iPSC) derived cells, will allow to study systemic effects under controlled physiological conditions at an unprecedented level of detail.

Acknowledgements

We are grateful to Nagabhooshan Hegde and the NIHS muscle aging group and community for discussion and support. We thank Phoukham Phothirath and Oliver Rizzo of the preclinical investigations group of Nestlé Research for expert advice and support with *in-vivo* experiments. O.M., J.N.F. and C.F.B are supported by the Fondation Suisse de Recherche sur les Maladies Musculaires (FSRMM). C.F.B. is supported by the Canadian Institutes of Health Research (PJT-162442), the Natural Sciences and Engineering Research Council of Canada (RGPIN-2017-05490), the Fonds de Recherche du Québec - Santé (Dossier 36789), the ThéCell Network (supported by the FRQS), the Canadian Stem Cell Network, and a research chair of the Centre de Recherche Médicale de l'Université de Sherbrooke (CRMUS). P.M.C is supported by ERC-2016-AdG-741966, La Caixa-HEALTH-HR17-00040, MDA, UPGRADE-H2020-825825, RTI2018-096068-B-I00. X.H is recipient of a Severo Ochoa FPI (SEV-2015-0505-17-1) predoctoral fellowship.

Author Contributions

O.M., X.H., C.B., F.D.F., J.M., and N.B. contributed to experimental design, conducted experiments and analyzed results. E.LM., J.C.T, J.I., and P.M.C. provided critical reagents and experimental support. E.M. performed bioinformatic analysis. S.M., F.R. and P.D. developed the RNA isolation methodology and performed transcriptional profiling. O.M., X.H., J.N.F, and C.F.B. directed the study, designed experiments, analyzed and interpreted results, and wrote the manuscript.

Competing Financial Interests

O.M., X.H., E.M., C.B., F.D.F., J.M., S.M., F.R., P.D., N.B., J.N.F. and C.F.B. were or are employees of the Société des Produits Nestlé S.A., Switzerland

Figure legends

Fig. 1 | PES hollow fiber capsules for transcriptomic profiling of long-range systemic signals. a, Scheme outlining interactions in the tissue niche in the context of the systemic circulation. Using cell encapsulation, the direct effects of long-range diffusible factors on maintenance and differentiation of defined cell types of interest can be assessed independent of the influence of accessory cells. **b**, Scanning electron micrographs of the polyethersulfone (PES) hollow fiber membrane. Scale bars: 200 μm (top left), 20 μm (bottom left) and 5 μm (right). **c**, Schematic outlining the capsule loading procedure and photograph of a PES hollow fiber membrane mounted to the adaptor hub.

Fig. 2 | *In-vitro* characterization of encapsulated myogenic progenitors. a,**b**, Terminal deoxynucleotidyl transferase dUTP nick end labeling (TUNEL) based quantification of apoptosis in encapsulated human (hskMP) or mouse (mskMP) skeletal muscle progenitors maintained in growth media for ten days. **c**,**d** DNA staining based quantification of hskMP or mskMP numbers in cross sections of capsules maintained for 4, 8 or 10 days in growth media. **e**,**f**, Representative DNA stainings of cross sections from a capsule containing hskMPs or mskMPs maintained ten days in growth media. Scale bars: 75 μm. **g**, Representative Pax7 immunostainings of cross sections from capsules containing hskMPs or mskMPs maintained ten days in growth media. Scale bars: 150 μm. **h**,**i**, Quantification of Pax7 positive cells in capsules containing hskMPs or mskMPs maintained for 4, 8 or 10 days in growth media. **j**, Representative MyoD immunostainings of cross sections from capsules containing hskMPs or mskMPs maintained ten days in growth media. Scale bars: 150 μm. **k**,**l**, Quantification of MyoD positive cells in capsules containing hskMPs or mskMPs maintained for 4, 8 or 10 days in growth media. **m-p**, Quantification of Pax7 and MyoD in cross sections from capsules maintained for four days under proliferative (Prolif.) conditions in growth media or in differentiation (Diff.) media. **q**, Representative myosin heavy chain (MHC) immunostainings of cross sections from capsules containing hskMPs or mskMPs maintained for four days in differentiation media. Scale bars: 75 μm. **r**,**s**, Quantification of MHC positive cells in capsules containing hskMPs or mskMPs maintained for four days in growth media compared to differentiation media. All graphs represent means +/- s.e.m. n≥3 cross sections from different capsules were quantified for each experiment and time-point. ****P<0.0001,

***P<0.001, **P<0.01, *P<0.05; Two-way comparisons were made with a student's t–test and multiple comparisons by one–way ANOVA followed by Bonferroni post–test.

Fig. 3 | *In-vivo* characterization of encapsulated myogenic progenitors. a, Schematic of the implantation strategy for the PES hollow fiber capsules in mice. In case of hskMPs, an osmotic pump supplying immunosuppressant was implanted at the contralateral flank. **b**, Photograph of the capsules in the connective tissue under the skin of mice ten days after implantation. Arrows are pointing at blood vessels in proximity of the capsules. **c**,**d**, Quantification of TUNEL negative hskMP or mskMP skeletal muscle progenitors after ten days *in-vivo*. **e**, Representative Pax7 immunostainings of cross sections from capsules containing hskMPs or mskMPs after ten days *in-vivo*. **f**,**g**, Quantification of Pax7 positive cells in capsules containing hskMPs or mskMPs after ten days *in-vivo*. **h**, Representative MyoD immunostainings of cross sections from capsules containing hskMPs or mskMPs after ten days *in-vivo*. **i**,**j**, Quantification of MyoD positive cells in capsules containing hskMPs or mskMPs after ten days *in-vivo*. **k**, Representative MHC immunostainings of cross sections from capsules containing hskMPs or mskMPs after ten days *in-vivo*. **l**,**m**, Quantification of MHC positive cells in capsules containing hskMPs or mskMPs after ten days *in-vivo* (**c**,**d**,**f**,**g**,**i**,**j**,**l**,**m**) Cross sections of capsules explanted from n=3 mice were analyzed for each experiment. Bars represent means +/- s.e.m. (**e**,**h**,**k**) Scale bars: 150 μm. Comparisons were made by one–way ANOVA followed by Bonferroni post–hoc test.

Fig. 4 | Transcriptomic profiling of systemic aging. a, Gene set enrichment analysis (GSEA) of age-induced genes in encapsulated hskMPs or mskMPs compared to the young control after ten days *in-vivo*. Shaded bars represent gene sets overlapping between human and mouse cells. **b**,**c**, GSEA barcode plots depicting enrichment of Myc targets with age in encapsulated hskMPs or mskMPs compared to the young control after ten days *in-vivo*. **d**, GSEA of genes downregulated with age in encapsulated hskMPs or mskMPs compared to the young control after ten days *in-vivo*. Shaded bars represent gene sets overlapping between human and mouse cells. **e**, GSEA of genes up- or downregulated with age in freshly isolated niche resident skeletal muscle stem cells. Shaded bars represent gene sets that are also changed with age in encapsulated hskMPs or mskMPs. Data from n=8 young or aged

mice. (**a-e**) Samples and data are derived from capsules of n≥5 mice in each age group. False discovery rate (FDR) = Adjusted p-value using Benjamini-Hochberg procedure.

Methods

Cell culture

Human skeletal myoblasts (Lonza, CC-2580) isolated from donated human tissue after obtaining permission for their use in research applications by informed consent and legal authorization were used at passages 3-5. For *in-vitro* expansion, the cells were maintained in human skeletal muscle myoblast growth medium (Zenbio, SKM-M) in a 37°C, 5% CO2 incubator, and were passaged once confluency reached 50%. Primary mouse myoblasts from 3-week-old C57Bl6/J (Charles River, C57BL/6NCrl) mice were maintained in Ham's F10 media (Wisent, 318-051-CL) containing 20% FBS (Wisent, 80450, lot 115714), 1% Penicillin-Streptomycin solution (Wisent, 450-201-EL) and 2,5 ng/mL bFGF (VWR, 10821-962) in a 37°C, 5% CO2 incubator at a confluence under 80%.

Embedding of cells

Growth factor reduced Matrigel (Corning, 354230) and MaxGel ECM (Sigma-Aldrich, E0282) were thawed at 4 °C and pipette tips were chilled at -20 °C before starting the experiment. All material was kept on ice or at 4 °C during the procedure. All mixing steps were carried out with caution to avoid generating bubbles. Cells were harvested with trypsin, numbers were quantified using a cell counter (Vi-CELL, AT39233), and the sample was centrifuged. The pellet was resuspended in ice-cold medium at a concentration of 20k cells/µl and kept on ice. The cell mixture was mixed with 1 volume Matrigel or MaxGel by gentle pipetting, giving rise to a final concentration of 10k cells/µl. Hydrogels (Sigma-Aldrich, TrueGel3D Hydrogel Kit, TRUE7) of ~10kPa were prepared by thawing of the SLO-DEXTRAN solution, TrueGel3D buffer at room temperature. SLO-DEXTRAN solution and TrueGel3D buffer were then mixed with the cells as described above for Matrigel and MaxGel. For hydrogel polymerization peptide based crosslinker (Sigma-Aldrich, TRUECD) was added to the cell suspension mix.

Device mounting

Polyethersulfone (PES) hollow fiber membranes (HFM, AKZO NOBEL) were cut into pieces of 1.2 cm (**Fig. 1b,c**). The adaptor hub (**Supplementary fig. 1d**) was produced by assembling a plastic loading head (Neurotech Pharmaceuticals) with a piece of PEBAX single lumen tubing (Medical Extrusion Technologies). The piece of HFM was then connected to the adaptor hub and sealed at the external interface and the exposed end using a bio-

compatible photopolymerizing medical grade adhesive (Loctite, Henkel, L37DAI9124). Polymerization was induced using a BlueWave LED Prime UVA high-intensity spot-curing system (Dymax, 40322) emitting two 5 second pulses of UV. The remaining empty lumen (1 cm) of the capsule holds a volume of 4 µL. Sealing of each device was verified using an air-leak test. While immerged in sterile double distilled water, filtered air was injected at a pressure of 17.58 hPa (2.5 Psi) for 5 s. Devices showing pressure decay greater than 100 Pa over 5 s were discarded. Assembled devices were sterilized with ethylene oxide gas before further use.

Cell encapsulation

10 µl of the cell-Matrigel mixture was loaded into each capsule using a Hamilton gastight syringe (50 µl) through the adaptor hub. Once the injected volume exceeded the inner volume of the device, a fraction of the total volume was ultrafiltrating through the porous membrane. The loaded capsule was transferred onto the 3D printed autoclavable USP Class VI plastic cutting and sealing platform (**Supplementary fig. 1e,f**), cut with a razor blade and sealed with the medical grade adhesive while left protected in the UV blocking plastic device. The capsule was then transferred to pre-warmed media and maintained on a shaker (80 rpm) in a 37° C, 5% CO2 incubator. Media was changed every day. For *in-vivo* studies, freshly loaded capsules were maintained in the incubator overnight before implantation. To re-isolate live cells from capsules, they were cut with a razor blade on both ends. A Hamilton gastight syringe was then used to perfuse with StemPro accutase (Thermo Fisher Scientific, A1110501).

Surgery

Capsule implantation experiments were performed using 6-week to 22-month-old male C57BL/6J mice (Janvier, C57BL/6JRj) in accordance with the Swiss regulation on animal experimentation and the European Community Council directive (86/609/EEC) for the care and use of laboratory animals. Experiments were approved by the Vaud cantonal authorities under license VD3085, and by the Animal Care and Ethics Committee of the Spanish National Cardiovascular Research Center (CNIC) and regional authorities. Mice had access to water and food ad libitum at all time. Before surgery, mice were anesthetized using isoflurane and lidocaine was applied onto the shaved skin. Capsules were implanted through

a small incision on the back, slightly posterior to the scapulae. Separated by 3-5 mm, 3-4 capsules were inserted through the incision into the subcutaneous fascia over the rip-cage using hypodermic venflon plastic tube (BD) sliding over a metal plunger. The metal plunger held the capsule in place while the plastic applicator tube was withdrawn over it. For encapsulated human cells, an osmotic minipump (Alzet 1002, Charles River) supplying 2.5 mg/kg/day of FK-506 in 70% ethanol (VWR Chemicals BDH, 153386F) was implanted through a second incision on the opposite side of the spine. Subsequently the incisions were closed using surgical staples. After surgery, mice were kept in single housing with daily surveillance and bodyweight measurement. 10 days after implantation, the mice were euthanized and the capsules were retrieved, washed in warm PBS, incubated in 37 °C warm trypsin for 5 minutes, and washed again before processing. Mice that showed weight loss >15% or displayed signs of wound infection and inflammation, were excluded from the study.

Cryo-sample preparation

Gelatin solution was heated up to and kept at 39 °C until completely melted. Capsules were placed on a layer of gelatin applied to a thin plastic mold. Subsequently, another layer of gelatin was applied to cover the capsules. The sample was then kept at 4 °C for 5 minutes to ensure complete gelation. The sample was then snap frozen in a liquid nitrogen chilled isopentane slurry for 1 minute and transferred to dry ice.

Stainings

Capsule cryosections were fixed with 4% PFA (Thermo Fisher Scientific, 28908). Fixed samples were washed with PBS and permeabilized in 0.1% Triton X-100 (Sigma-Aldrich, T8787) for 15 minutes at room temperature. The sections were then blocked with 4% IgG-free BSA (Jackson ImmunoResearch, 001000162) for 1 hour at room temperature. Samples were incubated with primary antibody at 4°C overnight or for 2 hours at room temperature in blocking buffer. After washing, the sections were incubated with the corresponding secondary antibodies and 40, 6-diamidino-2-phenylindole (Thermo Fisher Scientific, D1306) for 45 minutes at room temperature. After further washing, the slide was dried and mounted (ProLong Diamond Antifade Mountant, P36965). Imaging was carried out using a DMI6000 inverted microscope (Leica, DM14000B) or VS120 slide scanner (Olympus, EVK-L100-042FL). Primary antibodies were anti-Pax7 (DHSB, 528428), anti-MyoD antibody (C-20)

(Santa Cruz Biotechnology, sc-304) and anti-myosin heavy chain (Merck Millipore, A4.1025). TUNEL staining was performed using the *In-Situ* Cell Death Detection Kit (Roche, 11684795910) according to the manufacturer's instructions.

Fluorescence-activated cell sorting

Cells were isolated after 4 and 10 days of embedding into Matrigel, MaxGel and hydrogel using the TrypLE express enzyme (Thermo Fisher Scientific, 12605010) and StemPro accutase (Thermo Fisher Scientific, A1110501). Cell viability was determined using a LSRFortessa SORP FACS analyzer (BD Biosciences, H647800N0001). CytoCalcein (Pacific Blue) and Apopxin (FITC) (Abcam, ab176749) were used as indicators for live and apoptotic cells. Data was recorded with the BD FACSDiva software version 8.0.2. All data were subsequently analyzed with FCS Express Flow Cytometry version 6.06.0014 (De Novo Software, 4193).

Mouse inflammatory cytokines

Serum cytokines were quantified using the ELISA based Quantibody Mouse Inflammation Array Q1 Kit (Raybiotech, QAM-INF-1-1). Following incubation of the cytokine-specific immobilized antibodies with serum and standard cytokines, a biotinylated antibody cocktail recognizing the different bound cytokines was added. For detection, Cy3-labelled streptavidin was added, and fluorescence was quantified using the InnoScan 710 AL microarray scanner (Innopsys, Innoscan-710). Data was extracted and computed using MAPIX software (Innopsys, version 8.2.7) and Quantibody Q-Analyzer software (Raybiotech, QAM-INF-1-SW). Cytokine concentration in the samples was determined by comparing signals from unknown samples to the control cytokine standard curve.

RNA extraction and transcriptomic analysis

2-3 devices from the same mouse were pooled and added to a Lysing Matrix D tube (MP Biomedicals, 116913500) on ice. After addition of 450µL of Agencourt RNAdvance Tissue lysis buffer (Beckman Coulter, A32646) the capsules were homogenized using a FastPrep-24 (MP Biomedicals). RNA was extracted using the Agencourt RNAdvance Tissue Kit (Beckman Coulter, A32646) following the manufacturer's instructions. For encapsulated hskMPs, two rounds cRNA synthesis starting with 5 ng of total RNA were performed using the

MessageAmp II aRNA amplification kit (Life Technologies, AM1751) and MessageAmp II-biotin enhanced aRNA amplification kit (Life Technologies, AM1791) according to the manufacturer's instructions. RNA and cRNA were quantified using the Quant-iT RiboGreen RNA Assay Kit (Invitrogen, 10207502) using a Spectramax M2 (Molecular Devices, M2). RNA quality assessment was performed using a Bioanalyzer 2100 with RNA 6000 Pico Kit (Agilent Technologies, 5067-1513). cRNA quality assessment was done using a Fragment Analyzer-96 with the Standard Sensitivity RNA Analysis Kit (15-nt) (Advanced Analytical Technologies, DNF-471-0500). Hybridization of 750ng of cRNA on Human HT-12 v4.0 Expression BeadChip (Illumina, BD-103-0604), were performed according to the manufacturer's instructions. Scanning of the microarrays was performed on Illumina HiScan (Illumina, SY-103-1001). No signal was observed on human-specific microarrays using similar amounts of RNA/cRNA from connective tissue isolated in the immediate periphery of the implants. For encapsulated mskMPs, 50 ng of total-RNA was used to generate QuantSeq libraries using the QuantSeq-3' mRNA-Seq-Library Prep Kit FWD for Illumina (Lexogen, 15.384) following 20 cycles of PCR amplification. Libraries were quantified with the Quant-iT Picogreen (Invitrogen, 10545213) on a FilterMax F3 (Molecular Devices, F3). Size pattern was assessed with Fragment Analyzer-96 with the DNF-474-0500 High Sensitivity NGS Fragment Analysis Kit (Agilent Technologies, DNF-474-0500). Libraries (Average size: 295 bp) were pooled at an equimolar ratio and clustered at a concentration of 9 pM on a single read sequencing flow cell. 65 cycles of sequencing were performed on an Illumina HiSeq 2500 (Illumina, SY–401–2501) in rapid mode using a 50 cycles SBS Kit (Illumina, GD-402-4002, FC-402-4022) according to the manufacturer's instructions. The generated data were demultiplexed using bcl2fastq v2.19. Reads were aligned to the mouse genome (GRCm38) using STAR[47], and the number of reads mapped within genes was quantified by HTSeq[48]. Samples had a sequencing depth between 6.9-14.6 million reads, of which between 4.9-10.6 million reads were uniquely mapped. Freshly isolated niche resident cells were isolated and transcriptomically analyzed as previously described[49]. Briefly, extracted RNA were subjected to 3′ microarray analysis on Illumina MouseRef–8_V2 chips. For cross-referencing of data from encapsulated cells with the parabiosis study by Baruch et al[36], GO terms changed in encapsulated cells in the young and aged conditions were compared to the GO terms in clusters of genes differentially regulated in heterochronic vs isochronic parabionts in choroid plexus tissue (Baruch et al., figure S2B). Gene expression clusters in Baruch et al. were

generated based on K-means using Squared Euclidean distance as the correlation metrics.

3D-printing

Design of the capsule cutting-sealing platform was carried out using Solidworks software (Dassault Systèmes, SW PRO). Printing was done using the ProJet 3500 HDMax (3D systems) 3D printer. VisiJet M3 Crystal and VisiJet S300 (3D systems, 1.0000-M06 and 1.0000-M03) served as printing material and support material, respectively. Schematics are deposited on www.thingiverse.com/thing:4005301.

Statistical analysis

After visual inspection and exclusion of microarrays presenting low signal (log2 median expression <6) or low variability (standard deviation <0.1), Illumina expression signals were quantile-normalized. We applied a nonspecific filter to discard probes with low average signal and retained 6969 Illumina probes whose mean expression was greater than the third quartile of expression of all probes. Genes (represented by probes) were tested for differential expression using the moderated t-statistic as implemented in LIMMA[50]. RNA-sequencing data were normalized by the Trimmed Mean of M-values (TMM) method using the calcNormFactors function in edgeR[51] after selecting genes with more than 4 counts per-million in at least 5 samples. Differentially expressed genes were defined by fitting a quasi-likelihood negative binomial generalized log-linear model to count data using glmQLFTest function in edgeR. The mean-rank gene-set enrichment[52] procedure as implemented in LIMMA was applied to investigate pathway perturbations between gene profiles derived from encapsulated cells exposed to a young and aged environment using the hallmark and C5 (GO) gene set collections from MSigDB[53] version 6.2. All genome wide statistical analyses were performed using R, version 3.3.3 (microarray data), version 3.5.3 (RNA-sequencing data) and Bioconductor libraries. For cytokine arrays, the mean fluorescence intensities of positive controls were utilized for normalization. Values below the Limit of Detection (LOD) were substituted by LOD/sqrt(2) while the values above the highest standard were replaced by the highest standards. The non-parametric statistical (two-sample Wilcoxon) tests were used for the analysis. For visualization data were log-transformed.

Accession codes

The data discussed in this publication have been deposited in NCBI's Gene Expression

1 Omnibus and are accessible through GEO Series accession numbers GSE111401,
2 GSE00000 (under submission), GSE62762, and GSE81096.

References

1. Demontis, F., Piccirillo, R., Goldberg, A.L. et al. ***Aging Cell*** 12, 943 (2013).
2. Bert, P. ***J. Anatomie Physiologie*** 1, 69 (1864).
3. Conboy, I.M., Conboy, M.J. & Rebo, J. ***Aging (Albany NY)*** 7, 754 (2015).
4. Conboy, I.M., Conboy, M.J., Wagers, A.J. et al. ***Nature*** 433, 760 (2005).
5. Loffredo, F.S., Steinhauser, M.L., Jay, S.M. et al. ***Cell*** 153, 828 (2013).
6. Baht, G.S., Silkstone, D., Vi, L. et al. ***Nat Commun*** 6, 7131 (2015).
7. Sinha, M., Jang, Y.C., Oh, J. et al. ***Science*** 344, 649 (2014).
8. Villeda, S.A., Luo, J., Mosher, K.I. et al. ***Nature*** 477, 90 (2011).
9. Katsimpardi, L., Litterman, N.K., Schein, P.A. et al. ***Science*** 344, 630 (2014).
10. Smith, L.K., He, Y., Park, J.S. et al. ***Nat Med*** 21, 932 (2015).
11. Ruckh, J.M., Zhao, J.W., Shadrach, J.L. et al. ***Cell Stem Cell*** 10, 96 (2012).
12. Rebo, J., Mehdipour, M., Gathwala, R. et al. ***Nat Commun*** 7, 13363 (2016).
13. Conese, M., Carbone, A., Beccia, E. et al. ***Open Med (Wars)*** 12, 376 (2017).
14. Garcia, J.M., Merriam, G.R. & Kargi, A.Y. ***Endotext*** (2000).
15. ***Testosterone and Aging: Clinical Research Directions*** (2004).
16. Franceschi, C. & Campisi, J. ***J Gerontol A Biol Sci Med Sci*** 69 Suppl 1, S4 (2014).
17. Dominguez, L.J. & Barbagallo, M. ***Curr Opin Clin Nutr Metab Care*** 19, 5 (2016).
18. Yousef, H., Conboy, M.J., Morgenthaler, A. et al. ***Oncotarget*** 6, 11959 (2015).
19. Tanaka, T., Biancotto, A., Moaddel, R. et al. ***Aging Cell*** 17, e12799 (2018).
20. Lehallier, B., Gate, D., Schaum, N. et al. ***Nat Med*** 25, 1843 (2019).
21. Conboy, I.M. & Rando, T.A. ***Dev Cell*** 3, 397 (2002).
22. Castellano, J.M., Mosher, K.I., Abbey, R.J. et al. ***Nature*** 544, 488 (2017).
23. Mahmoudi, S., Xu, L. & Brunet, A. ***Nat Cell Biol*** 21, 32 (2019).
24. Yilmaz, O.H., Katajisto, P., Lamming, D.W. et al. ***Nature*** 486, 490 (2012).
25. Biferali, B., Proietti, D., Mozzetta, C. et al. ***Front Physiol*** 10, 1074 (2019).
26. Lukjanenko, L., Karaz, S., Stuelsatz, P. et al. ***Cell Stem Cell*** (2019).
27. Smith, L.K., White, C.W., 3rd & Villeda, S.A. ***Cell Tissue Res*** 371, 105 (2018).
28. Zhao, C., Xue, J., Ran, F. et al. ***Progress in Materials Science*** 58, 76 (2013).
29. Hunter, S.K., Kao, J.M., Wang, Y. et al. ***ASAIO J*** 45, 37 (1999).
30. Kleinman, H.K., McGarvey, M.L., Liotta, L.A. et al. ***Biochemistry*** 21, 6188 (1982).
31. Hofmann, J.W., Zhao, X., De Cecco, M. et al. ***Cell*** 160, 477 (2015).
32. Shavlakadze, T., Zhu, J., Wang, S. et al. ***J Gerontol A Biol Sci Med Sci*** 73, 845 (2018).
33. Dimri, G.P., Itahana, K., Acosta, M. et al. ***Mol Cell Biol*** 20, 273 (2000).
34. Liu, T., Zhou, Y., Ko, K.S. et al. ***Mediators Inflamm*** 2015, 276850 (2015).
35. Frank, S.R., Schroeder, M., Fernandez, P. et al. ***Genes Dev*** 15, 2069 (2001).
36. Baruch, K., Deczkowska, A., David, E. et al. ***Science*** 346, 89 (2014).
37. Lathuiliere, A., Cosson, S., Lutolf, M.P. et al. ***Biomaterials*** 35, 779 (2014).
38. Zhao, C.S., Liu, T., Lu, Z.P. et al. ***Artif Organs*** 25, 60 (2001).
39. Tullis, R.H., Duffin, R.P., Zech, M. et al. ***Ther Apher*** 6, 213 (2002).
40. Samtleben, W., Dengler, C., Reinhardt, B. et al. ***Nephrol Dial Transplant*** 18, 2382 (2003).
41. Werner, C., Jacobasch, H.J. & Reichelt, G. ***J Biomater Sci Polym Ed*** 7, 61 (1995).
42. Evano, B. & Tajbakhsh, S. ***NPJ Regen Med*** 3, 24 (2018).
43. Gopinath, S.D. & Rando, T.A. ***Aging Cell*** 7, 590 (2008).

44. Drew, L. ***Nature*** 555, S15 (2018).
45. Montecino-Rodriguez, E., Berent-Maoz, B. & Dorshkind, K. ***J Clin Invest*** 123, 958 (2013).
46. Franceschi, C., Capri, M., Monti, D. et al. ***Mech Ageing Dev*** 128, 92 (2007).
47. Dobin, A., Davis, C.A., Schlesinger, F. et al. ***Bioinformatics*** 29, 15 (2013).
48. Anders, S., Pyl, P.T. & Huber, W. ***Bioinformatics*** 31, 166 (2015).
49. Lukjanenko, L., Jung, M.J., Hegde, N. et al. ***Nat Med*** 22, 897 (2016).
50. Smyth, G.K. ***Stat Appl Genet Mol Biol*** 3, Article3 (2004).
51. Robinson, M.D., McCarthy, D.J. & Smyth, G.K. ***Bioinformatics*** 26, 139 (2010).
52. Michaud, J., Simpson, K.M., Escher, R. et al. ***BMC Genomics*** 9, 363 (2008).
53. Liberzon, A., Birger, C., Thorvaldsdottir, H. et al. ***Cell Syst*** 1, 417 (2015).

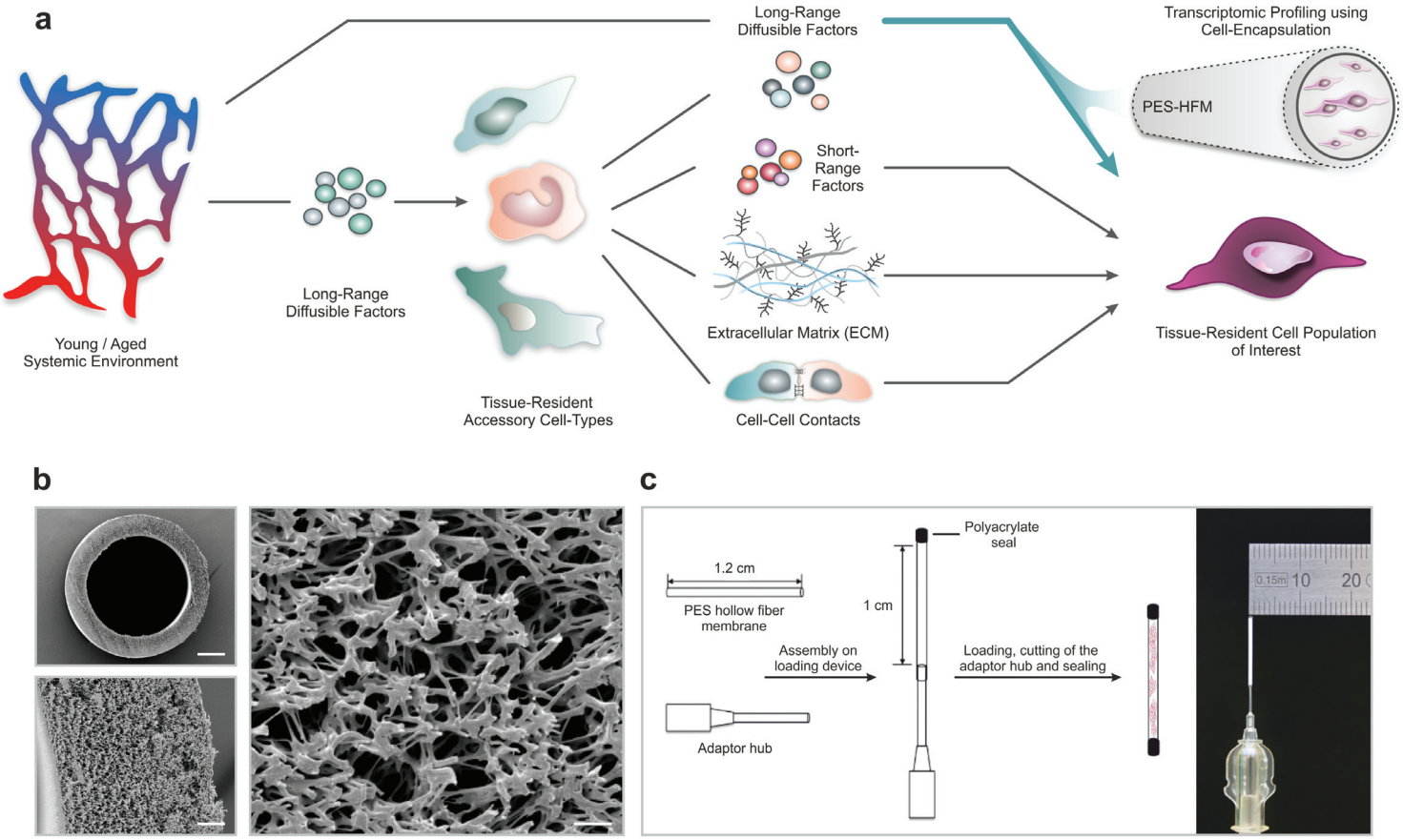
a
Young / Aged
Systemic Environment
Long-Range
Diffusible Factors
Tissue-Resident
Accessory Cell-Types
Long-Range
Diffusible Factors
Short-
Range
Factors
Extracellular Matrix (ECM)
Cell-Cell Contacts
Transcriptomic Profiling using
Cell-Encapsulation
PES-HFM
Tissue-Resident Cell Population
of Interest
b
c
1.2 cm
PES hollow fiber
membrane
Assembly on
loading device
Adaptor hub
1 cm
Polyacrylate
seal
Loading, cutting of the
adaptor hub and sealing

Figure 1

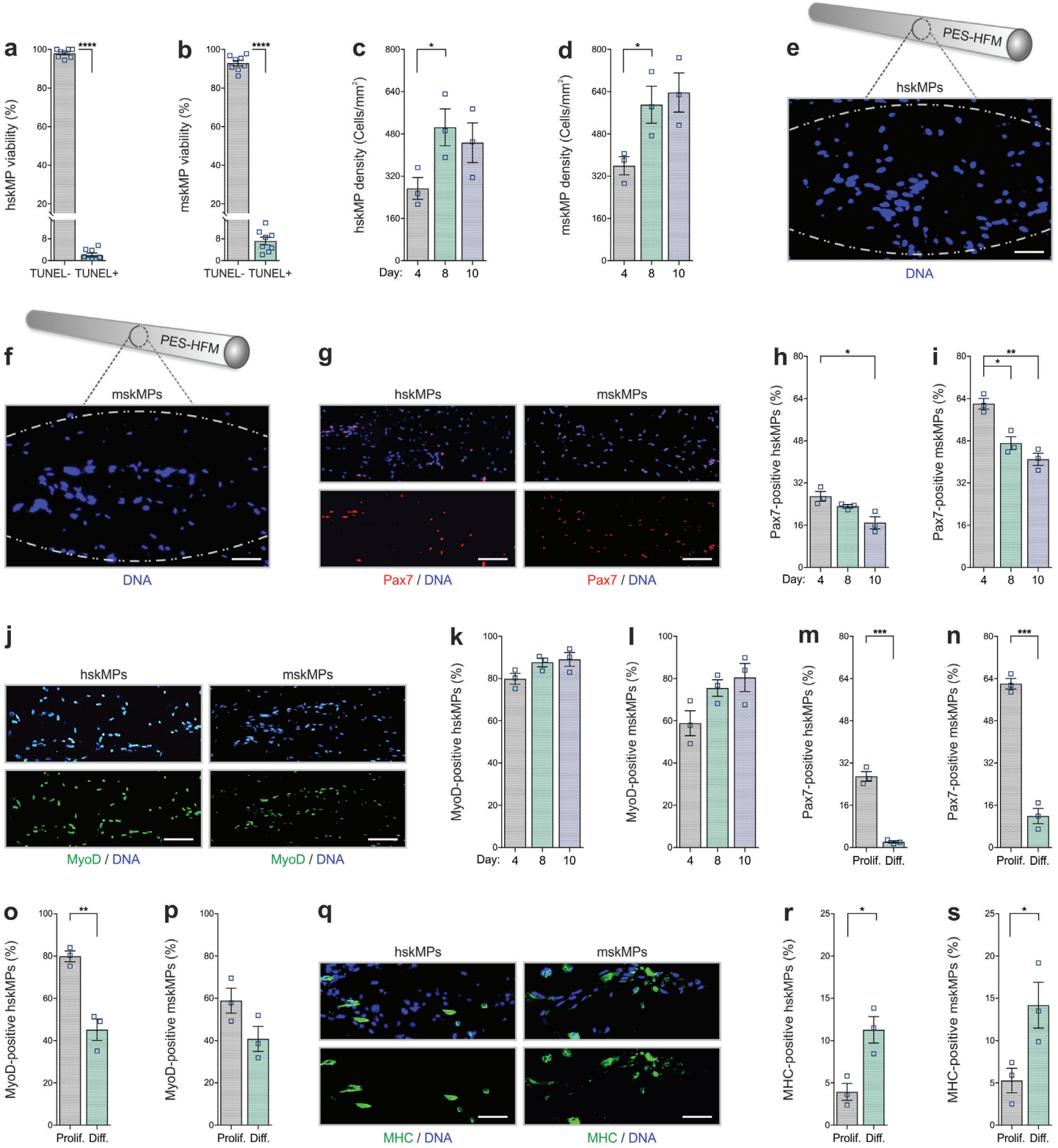
a
hskMP viability (%)
TUNEL- TUNEL+
****
b
mskMP viability (%)
TUNEL- TUNEL+
****
c
hskMP density (Cells/mm²)
Day: 4 8 10
*
d
mskMP density (Cells/mm²)
4 8 10
*
e
PES-HFM
hskMPs
DNA
f
PES-HFM
mskMPs
DNA
g
hskMPs
mskMPs
Pax7 / DNA
Pax7 / DNA
h
Pax7-positive hskMPs (%)
Day: 4 8 10
*
i
Pax7-positive mskMPs (%)
4 8 10
*
**
j
hskMPs
mskMPs
MyoD / DNA
MyoD / DNA
k
MyoD-positive hskMPs (%)
Day: 4 8 10
l
MyoD-positive mskMPs (%)
4 8 10
m
Pax7-positive hskMPs (%)
Prolif. Diff.
***
n
Pax7-positive mskMPs (%)
Prolif. Diff.
***
o
MyoD-positive hskMPs (%)
Prolif. Diff.
**
p
MyoD-positive mskMPs (%)
Prolif. Diff.
q
hskMPs
mskMPs
MHC / DNA
MHC / DNA
r
MHC-positive hskMPs (%)
Prolif. Diff.
*
s
MHC-positive mskMPs (%)
Prolif. Diff.
*

Figure 2

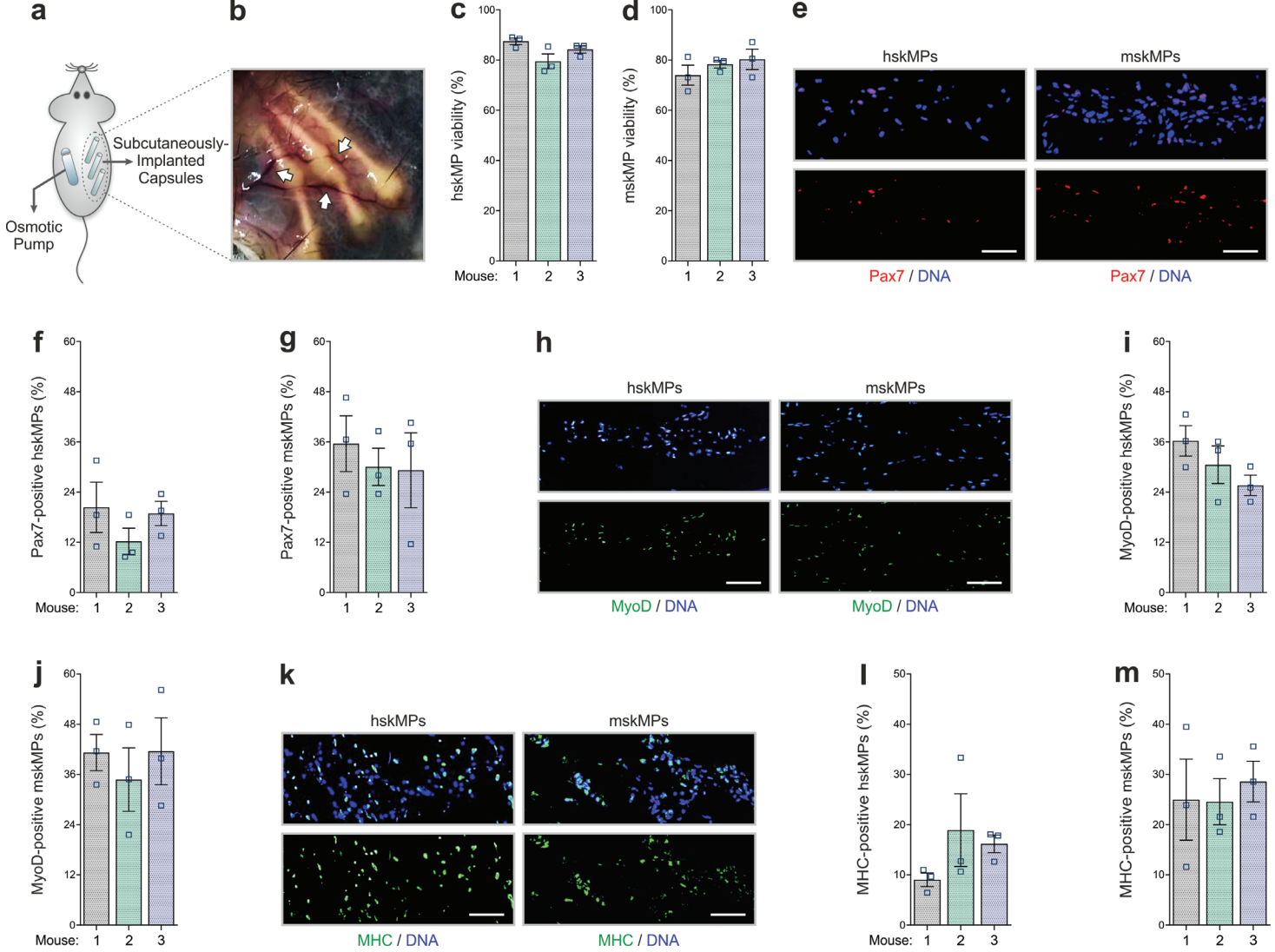
a
Subcutaneously-Implanted Capsules
Osmotic Pump
b
c
hskMP viability (%)
Mouse: 1 2 3
d
mskMP viability (%)
e
hskMPs
mskMPs
Pax7 / DNA
Pax7 / DNA
f
Pax7-positive hskMPs (%)
Mouse: 1 2 3
g
Pax7-positive mskMPs (%)
h
hskMPs
mskMPs
MyoD / DNA
MyoD / DNA
i
MyoD-positive hskMPs (%)
Mouse: 1 2 3
j
MyoD-positive mskMPs (%)
Mouse: 1 2 3
k
hskMPs
mskMPs
MHC / DNA
MHC / DNA
l
MHC-positive hskMPs (%)
Mouse: 1 2 3
m
MHC-positive mskMPs (%)

Figure 3

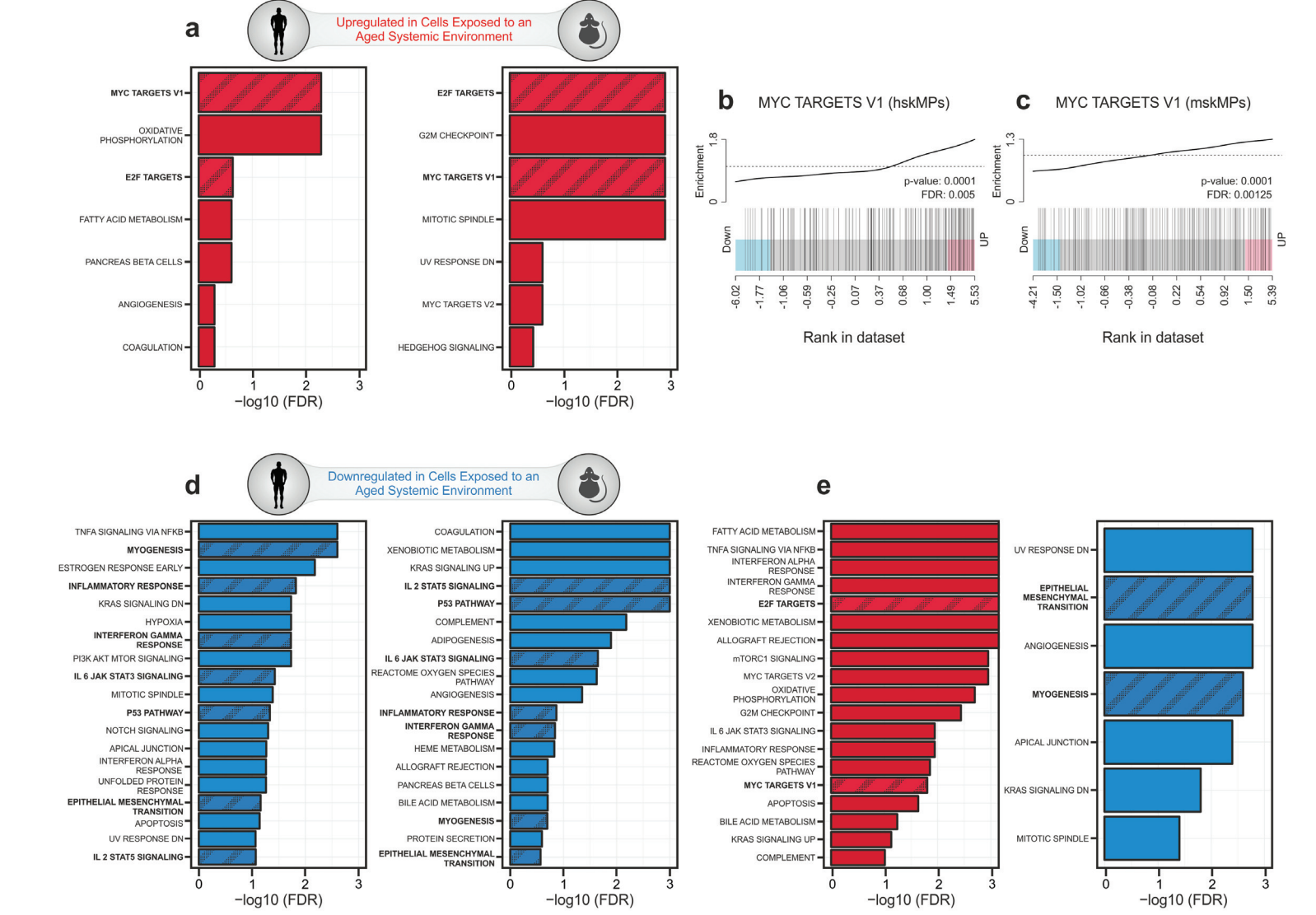
a
Upregulated in Cells Exposed to an Aged Systemic Environment
MYC TARGETS V1
OXIDATIVE PHOSPHORYLATION
E2F TARGETS
FATTY ACID METABOLISM
PANCREAS BETA CELLS
ANGIOGENESIS
COAGULATION
E2F TARGETS
G2M CHECKPOINT
MYC TARGETS V1
MITOTIC SPINDLE
UV RESPONSE DN
MYC TARGETS V2
HEDGEHOG SIGNALING
−log10 (FDR)
b
MYC TARGETS V1 (hskMPs)
Enrichment
p-value: 0.0001
FDR: 0.005
Down
UP
Rank in dataset
c
MYC TARGETS V1 (mskMPs)
p-value: 0.0001
FDR: 0.00125
d
Downregulated in Cells Exposed to an Aged Systemic Environment
TNFA SIGNALING VIA NFKB
MYOGENESIS
ESTROGEN RESPONSE EARLY
INFLAMMATORY RESPONSE
KRAS SIGNALING DN
HYPOXIA
INTERFERON GAMMA RESPONSE
PI3K AKT MTOR SIGNALING
IL 6 JAK STAT3 SIGNALING
MITOTIC SPINDLE
P53 PATHWAY
NOTCH SIGNALING
APICAL JUNCTION
INTERFERON ALPHA RESPONSE
UNFOLDED PROTEIN RESPONSE
EPITHELIAL MESENCHYMAL TRANSITION
APOPTOSIS
UV RESPONSE DN
IL 2 STAT5 SIGNALING
COAGULATION
XENOBIOTIC METABOLISM
KRAS SIGNALING UP
IL 2 STAT5 SIGNALING
P53 PATHWAY
COMPLEMENT
ADIPOGENESIS
IL 6 JAK STAT3 SIGNALING
REACTOME OXYGEN SPECIES PATHWAY
ANGIOGENESIS
INFLAMMATORY RESPONSE
INTERFERON GAMMA RESPONSE
HEME METABOLISM
ALLOGRAFT REJECTION
PANCREAS BETA CELLS
BILE ACID METABOLISM
MYOGENESIS
PROTEIN SECRETION
EPITHELIAL MESENCHYMAL TRANSITION
e
FATTY ACID METABOLISM
TNFA SIGNALING VIA NFKB
INTERFERON ALPHA RESPONSE
INTERFERON GAMMA RESPONSE
E2F TARGETS
XENOBIOTIC METABOLISM
ALLOGRAFT REJECTION
mTORC1 SIGNALING
MYC TARGETS V2
OXIDATIVE PHOSPHORYLATION
G2M CHECKPOINT
IL 6 JAK STAT3 SIGNALING
INFLAMMATORY RESPONSE
REACTOME OXYGEN SPECIES PATHWAY
MYC TARGETS V1
APOPTOSIS
BILE ACID METABOLISM
KRAS SIGNALING UP
COMPLEMENT
UV RESPONSE DN
EPITHELIAL MESENCHYMAL TRANSITION
ANGIOGENESIS
MYOGENESIS
APICAL JUNCTION
KRAS SIGNALING DN
MITOTIC SPINDLE
−log10 (FDR)

Figure 4

In-vivo Transcriptomic Profiling of Systemic Aging using Cell Encapsulation

Omid Mashinchian, Xiaotong Hong, Eugenia Migliavacca, Christophe Boss, Filippo De Franceschi, Joris Michaud, Emmeran Le Moal, Jasmin Collerette-Tremblay, Joan Isern, Sylviane Metairon, Frederic Raymond, Patrick Descombes, Nicolas Bouche, Pura Muñoz-Cánoves, Jerome N. Feige, C. Florian Bentzinger

Supplementary Information

Supplementary Figures 1-4
Supplementary Table 1-10

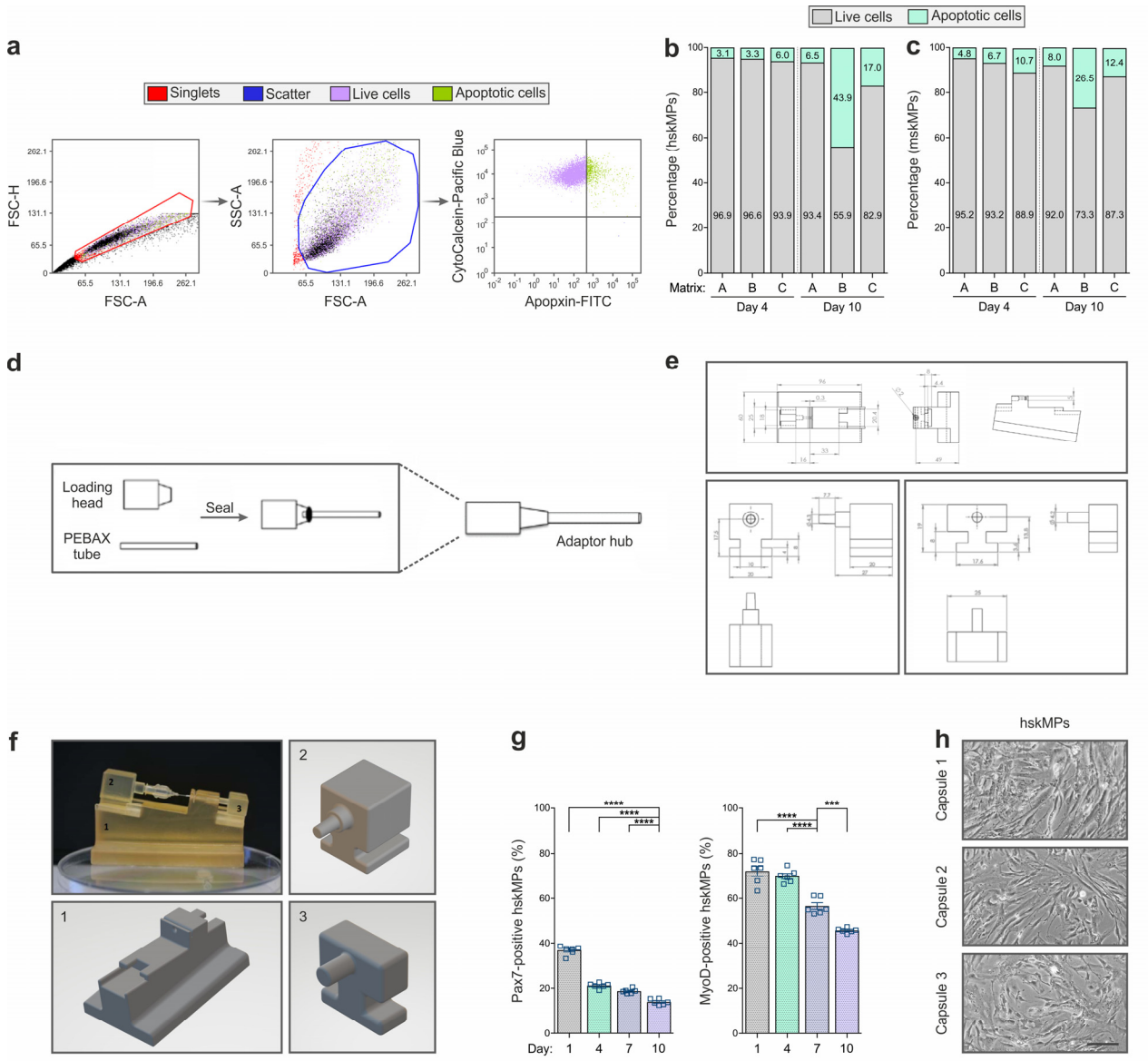
a
Singlets
Scatter
Live cells
Apoptotic cells
FSC-H
FSC-A
SSC-A
CytoCalcein-Pacific Blue
Apopxin-FITC
b
Live cells
Apoptotic cells
Percentage (hskMPs)
Matrix:
Day 4
Day 10
c
Percentage (mskMPs)
d
Loading head
PEBAX tube
Seal
Adaptor hub
e
f
g
Pax7-positive hskMPs (%)
MyoD-positive hskMPs (%)
Day:
h
hskMPs
Capsule 1
Capsule 2
Capsule 3

Supplementary fig. 1 | a, Flow cytometry strategy used to identify live and apoptotic cells. CytoCalcein is sequestered in the cytoplasm of live cells, while apoptosis is measured by labeling of cell surface phosphatidylserine using Apopxin. **b**, Quantification of live and apoptotic human (hskMP) or mouse (mskMP) skeletal muscle progenitors embedded into different biomaterials and maintained in growth media for four or ten days. A=Growth factor reduced Matrigel, B=Hydrogel, C=MaxGel extracellular matrix. Values were obtained from pooled cells of n=6 replicates. **c**, Schematic outlining the construction of the adaptor hub used for mounting and loading of the capsules. **d**,**e**, Schematics and graphical representations of the parts of the 3D printed capsule cutting and sealing platform. The photograph in the upper left of (**f**) shows the assembled platform loaded with a capsule mounted to the adaptor hub. **g**, Quantification of Pax7 and MyoD positive hskMPs over a time course of ten days in 2D culture. Graphs represent means +/- s.e.m. n=6 replicates for each time-point. ****P<0.0001, ***P<0.001; One–way ANOVA followed by Bonferroni post–test. **h**, Representative bright field images of hskMPs in 2D culture after enzymatic liberation following ten days of encapsulation. Scalebar = 40 μm.

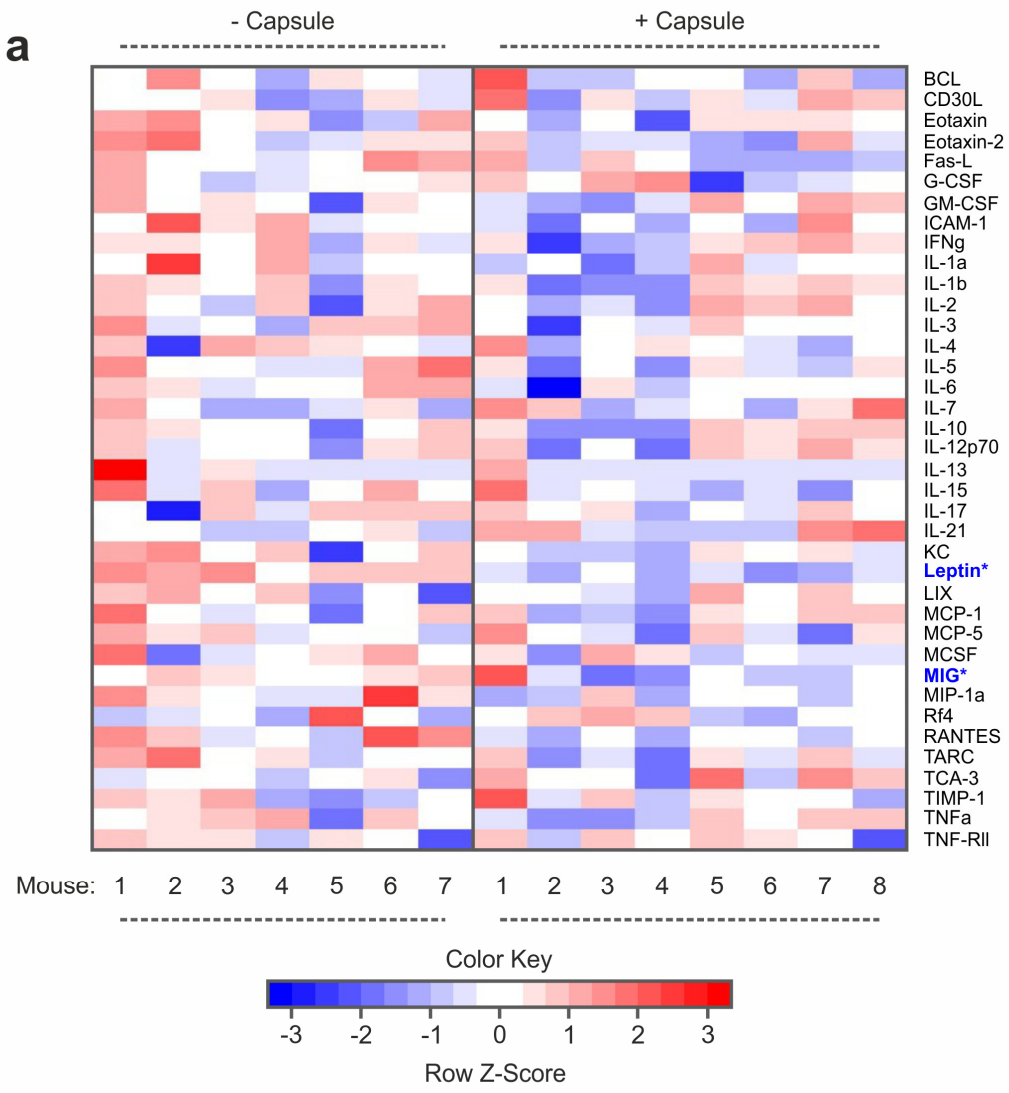

Supplementary fig. 2 | a, Multiplexed enzyme-linked immunosorbent assay (ELISA) array signal heatmaps for levels of inflammatory factors in serum of mice that underwent surgical implantation of PES hollow fiber capsules compared to untreated controls ten days after the procedure. n≥7 mice. Asterisks indicate factors changed with a p-value of ≤0.05 in a two-sample Wilcoxon test. TNF-RI and MIP-1g were excluded from the analysis since signals were outside of the detection range.

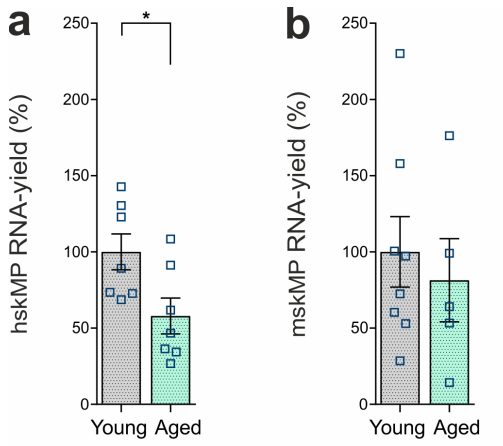

Supplementary fig. 3 | a,**b** RNA yield from capsules containing hskMPs or mskMPs after ten days in-vivo in young and aged mice. For each replicate two capsules from one mouse were pooled. Bars represent means +/- s.e.m. Data is derived from capsules of n≥5 mice in each group. *P<0.05 in a student's t–test.

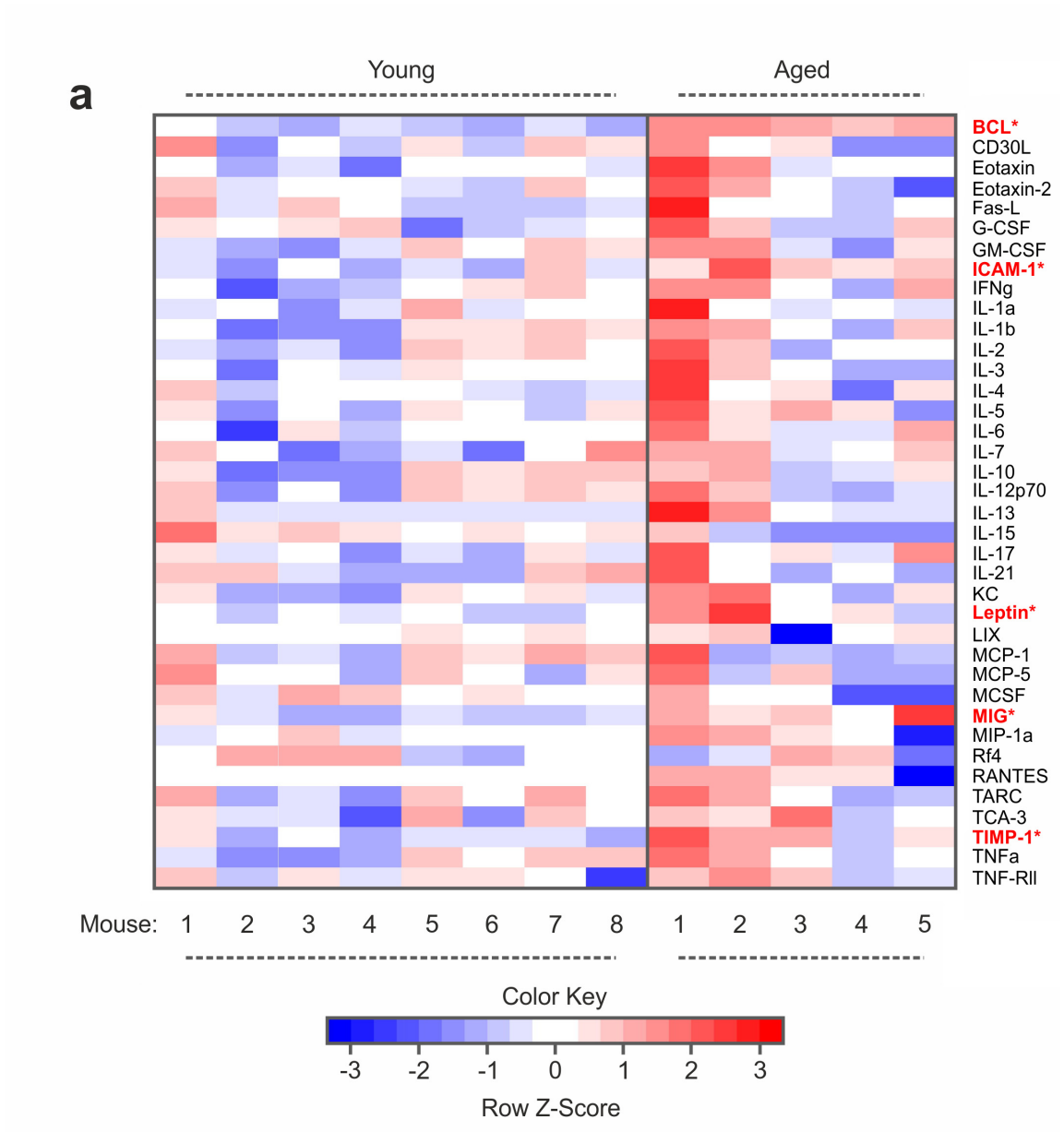

Supplementary fig. 4 | a, Multiplexed ELISA array heatmaps for levels of inflammatory factors in plasma of young and aged mice. n≥5 mice. Asterisks indicate factors changed with a p-value of ≤0.05 in a two-sample Wilcoxon test. TNF-RI and MIP-1g were excluded from the analysis since signals were outside of the detection range.

	- Capsule							+ Capsule							
Mouse	**1**	**2**	**3**	**4**	**5**	**6**	**7**	**1**	**2**	**3**	**4**	**5**	**6**	**7**	**8**
BLC	18.5	28.5	20.5	14.4	23.0	18.6	18.2	33.6	16.7	16.3	21.3	21.2	15.1	24.0	15.1
CD30L	11.2	9.4	13.9	1.1	5.4	13.3	8.2	35.2	3.1	13.2	6.7	15.2	6.9	21.8	18.8
Eotaxin	312.8	344.3	183.5	240.3	122.8	159.1	302.6	213.1	139.2	181.6	92.7	253.5	250.7	245.6	192.2
Eotaxin-2	165.7	212.9	96.7	63.6	80.9	107.4	118.4	125.8	66.0	71.5	72.6	57.8	52.9	153.6	78.4
Fas L	115.4	17.8	30.8	13.0	36.4	119.8	92.0	100.6	11.1	77.1	25.6	0.0	1.6	6.0	9.1
G-CSF	219.4	168.9	113.9	126.1	160.7	145.1	186.4	211.0	156.4	229.1	255.7	62.7	118.5	130.1	145.6
GM-CSF	26.2	20.3	21.3	19.2	9.9	21.7	20.6	16.1	12.6	12.0	16.2	27.0	19.2	27.2	25.3
ICAM-1	1873.4	2621.3	2061.8	2268.4	1723.5	1824.2	1947.8	1765.7	1440.2	1896.0	1588.8	1871.7	1597.9	2409.4	1874.0
IFNg	66.7	65.9	63.8	85.6	39.0	69.7	51.2	67.5	25.4	40.0	43.0	68.1	78.2	85.5	65.4
IL-1a	4.6	17.0	5.3	8.4	2.7	4.4	4.6	3.0	3.8	1.6	2.9	8.0	3.3	4.8	4.8
IL-1b	171.3	164.0	143.3	183.4	77.5	149.3	123.9	156.0	72.4	83.5	80.2	175.8	167.0	185.9	162.6
IL-2	116.4	91.6	77.9	116.6	57.5	106.1	122.5	88.0	74.8	84.9	69.0	123.7	114.0	121.2	97.2
IL-3	3.8	1.1	1.5	0.8	2.6	2.7	3.3	1.8	0.3	1.4	1.1	2.4	1.5	1.4	1.7
IL-4	2.2	0.0	2.8	2.3	1.9	1.6	1.1	3.6	0.8	1.7	1.9	1.5	1.1	0.8	1.3
IL-5	131.3	71.0	79.2	69.2	66.4	111.7	156.0	91.7	43.6	75.2	48.7	92.8	69.7	59.0	92.5
IL-6	23.6	19.5	11.3	16.4	14.4	25.3	25.8	11.9	3.0	17.9	9.7	17.0	14.7	14.6	15.9
IL-7	87.3	46.8	0.0	9.5	21.8	56.3	10.0	116.5	65.8	3.6	27.9	38.0	0.0	65.7	194.5
IL-10	324.7	307.3	261.2	272.0	119.3	262.4	309.6	287.5	139.5	147.3	142.0	340.5	292.4	316.5	323.1
IL-12p70	93.2	56.1	72.5	62.3	38.2	85.3	96.0	100.3	37.2	65.8	36.6	96.6	84.2	107.1	88.8
IL-13	171.3	6.2	18.5	4.8	4.5	0.0	0.0	31.4	0.0	0.9	6.4	0.0	0.0	3.1	0.0
IL-15	479.5	136.3	265.4	107.0	194.8	360.8	161.7	482.5	138.8	202.3	153.6	105.6	145.8	81.5	168.7
IL-17	2.1	0.1	4.0	1.2	3.6	3.5	4.1	3.6	1.7	2.7	0.9	2.0	1.2	3.6	1.8
IL-21	5.7	5.6	0.0	0.0	5.8	8.5	1.8	15.1	14.4	4.0	0.0	0.0	0.0	15.5	20.1
KC	4.6	4.8	3.6	4.4	2.0	3.3	4.4	3.7	2.9	2.9	2.7	3.9	3.5	3.9	3.2
Leptin	661.5	586.4	665.4	296.8	428.9	414.8	432.2	140.3	91.7	188.0	105.9	161.8	78.7	83.4	161.9
LIX	508.7	553.1	377.6	460.3	215.1	379.6	153.0	356.0	322.0	292.9	230.1	531.1	381.0	482.4	392.8
MCP-1	59.6	30.9	24.2	29.9	15.9	30.2	42.2	45.0	20.3	21.4	16.8	37.7	32.9	45.0	40.9
MCP-5	47.9	32.3	36.4	21.6	29.4	30.1	18.9	53.2	25.8	19.8	11.6	40.9	20.9	11.1	31.4
MCSF	9.6	0.7	1.9	3.4	4.1	7.2	2.6	4.3	0.8	6.1	3.7	1.5	3.1	2.0	1.7
MIG	41.0	49.3	45.0	40.9	42.3	43.7	46.2	67.0	35.5	25.7	28.1	36.9	31.8	32.8	40.9
MIP-1a	24.1	16.1	13.9	12.2	11.6	36.7	16.8	8.4	10.3	19.6	8.9	12.8	12.6	10.8	12.5
PF4	3066.6	3415.4	3692.6	3006.8	5273.3	3779.9	2905.3	3734.5	4274.5	4317.3	4222.6	3164.9	2978.8	3612.0	3644.5
RANTES	3.2	2.6	1.7	1.8	1.5	4.3	3.3	1.7	1.3	2.2	1.4	2.1	1.8	1.5	1.8
TARC	40.9	48.3	26.0	31.1	18.4	26.9	23.0	35.2	14.0	19.5	12.1	30.0	20.1	36.6	20.7
TCA-3	18.0	19.5	21.4	14.9	21.0	26.6	11.1	34.7	23.5	23.3	10.4	45.4	14.2	38.8	30.2
TIMP-1	597.3	575.2	638.2	442.1	431.9	456.9	512.9	721.0	479.6	587.1	472.9	563.8	544.4	555.8	445.5
TNFa	29.8	37.4	41.9	48.4	17.0	43.1	34.8	28.0	19.2	18.2	22.7	44.8	34.4	42.6	44.5
TNF RII	412.8	370.1	350.4	196.1	348.9	267.6	116.9	416.2	209.0	373.4	259.0	396.6	367.6	306.4	113.3

Supplementary table 1 | Multiplexed ELISA quantification of inflammatory factors in serum of mice that underwent surgical implantation of PES hollow fiber capsules compared to untreated controls ten days after the procedure. n≥7 mice. Each value represents averages in pg/ml from n=4 technical replicates for each factor. TNF-RI and MIP-1g were excluded from the analysis since signals were outside of the detection range.

Gene Set Name - Human	GST Pval	GST FDR
HALLMARK_MYC_TARGETS_V1	1.00E-04	0.005
HALLMARK_OXIDATIVE_PHOSPHORYLATION	2.00E-04	0.005
HALLMARK_E2F_TARGETS	0.0166	0.238
HALLMARK_FATTY_ACID_METABOLISM	0.0215	0.238
HALLMARK_PANCREAS_BETA_CELLS	0.0238	0.238
HALLMARK_ANGIOGENESIS	0.0648	0.506428571
HALLMARK_COAGULATION	0.0709	0.506428571
HALLMARK_KRAS_SIGNALING_UP	0.1885	1
HALLMARK_XENOBIOTIC_METABOLISM	0.1988	1
HALLMARK_ADIPOGENESIS	0.2427	1
HALLMARK_G2M_CHECKPOINT	0.2755	1
HALLMARK_REACTIVE_OXIGEN_SPECIES_PATHWAY	0.284	1
HALLMARK_SPERMATOGENESIS	0.3227	1
HALLMARK_ANDROGEN_RESPONSE	0.3554	1
HALLMARK_WNT_BETA_CATENIN_SIGNALING	0.3626	1
HALLMARK_PROTEIN_SECRETION	0.4046	1
HALLMARK_CHOLESTEROL_HOMEOSTASIS	0.5342	1
HALLMARK_MYC_TARGETS_V2	0.633	1
HALLMARK_BILE_ACID_METABOLISM	0.6826	1
HALLMARK_HEME_METABOLISM	0.7257	1
HALLMARK_TGF_BETA_SIGNALING	0.7263	1
HALLMARK_PEROXISOME	0.7279	1
HALLMARK_DNA_REPAIR	0.7765	1
HALLMARK_ALLOGRAFT_REJECTION	0.788	1
HALLMARK_MTORC1_SIGNALING	0.9169	1
HALLMARK_UV_RESPONSE_UP	0.9296	1
HALLMARK_APICAL_SURFACE	0.9408	1
HALLMARK_HEDGEHOG_SIGNALING	0.9426	1
HALLMARK_ESTROGEN_RESPONSE_LATE	0.9434	1
HALLMARK_IL2_STAT5_SIGNALING	0.961	1
HALLMARK_GLYCOLYSIS	0.963	1
HALLMARK_COMPLEMENT	0.964	1
HALLMARK_UV_RESPONSE_DN	0.9709	1
HALLMARK_APOPTOSIS	0.9756	1
HALLMARK_EPITHELIAL_MESENCHYMAL_TRANSITION	0.979	1
HALLMARK_INTERFERON_ALPHA_RESPONSE	0.9823	1
HALLMARK_UNFOLDED_PROTEIN_RESPONSE	0.9841	1
HALLMARK_APICAL_JUNCTION	0.9851	1
HALLMARK_NOTCH_SIGNALING	0.9871	1
HALLMARK_P53_PATHWAY	0.9898	1
HALLMARK_MITOTIC_SPINDLE	0.9913	1
HALLMARK_IL6_JAK_STAT3_SIGNALING	0.992	1
HALLMARK_PI3K_AKT_MTOR_SIGNALING	0.9961	1
HALLMARK_INTERFERON_GAMMA_RESPONSE	0.9976	1
HALLMARK_KRAS_SIGNALING_DN	0.9978	1
HALLMARK_HYPOXIA	0.9986	1
HALLMARK_INFLAMMATORY_RESPONSE	0.9988	1
HALLMARK_ESTROGEN_RESPONSE_EARLY	0.9996	1
HALLMARK_TNFA_SIGNALING_VIA_NFKB	0.9998	1
HALLMARK_MYOGENESIS	1	1

Supplementary table 2 | Gene sets increased with age in encapsulated hskMPs compared to the young control after ten days *in-vivo*. GST Pval = Wilcoxon gene set test p- value. GST FDR = Adjusted p-value using the Benjamini-Hochberg procedure. GST FDR = Wilcoxon gene set test false discovery rate.

Gene Set Name - Mouse	GST Pval	GST FDR
HALLMARK_MITOTIC_SPINDLE	1.00E-04	0.00125
HALLMARK_G2M_CHECKPOINT	1.00E-04	0.00125
HALLMARK_E2F_TARGETS	1.00E-04	0.00125
HALLMARK_MYC_TARGETS_V1	1.00E-04	0.00125
HALLMARK_UV_RESPONSE_DN	0.0271	0.245833333
HALLMARK_MYC_TARGETS_V2	0.0295	0.245833333
HALLMARK_HEDGEHOG_SIGNALING	0.0512	0.365714286
HALLMARK_CHOLESTEROL_HOMEOSTASIS	0.1214	0.677777778
HALLMARK_KRAS_SIGNALING_DN	0.122	0.677777778
HALLMARK_NOTCH_SIGNALING	0.1655	0.8275
HALLMARK_TGF_BETA_SIGNALING	0.2272	1
HALLMARK_APICAL_JUNCTION	0.3936	1
HALLMARK_PI3K_AKT_MTOR_SIGNALING	0.4044	1
HALLMARK_ANDROGEN_RESPONSE	0.4386	1
HALLMARK_FATTY_ACID_METABOLISM	0.5445	1
HALLMARK_OXIDATIVE_PHOSPHORYLATION	0.5468	1
HALLMARK_MTORC1_SIGNALING	0.6076	1
HALLMARK_ESTROGEN_RESPONSE_LATE	0.653	1
HALLMARK_SPERMATOGENESIS	0.6719	1
HALLMARK_TNFA_SIGNALING_VIA_NFKB	0.712	1
HALLMARK_APICAL_SURFACE	0.7926	1
HALLMARK_INTERFERON_ALPHA_RESPONSE	0.7937	1
HALLMARK_UNFOLDED_PROTEIN_RESPONSE	0.8104	1
HALLMARK_APOPTOSIS	0.8208	1
HALLMARK_PEROXISOME	0.823	1
HALLMARK_HYPOXIA	0.8294	1
HALLMARK_WNT_BETA_CATENIN_SIGNALING	0.8509	1
HALLMARK_DNA_REPAIR	0.8616	1
HALLMARK_UV_RESPONSE_UP	0.8777	1
HALLMARK_ESTROGEN_RESPONSE_EARLY	0.8856	1
HALLMARK_GLYCOLYSIS	0.8878	1
HALLMARK_EPITHELIAL_MESENCHYMAL_TRANSITION	0.8937	1
HALLMARK_PROTEIN_SECRETION	0.9015	1
HALLMARK_MYOGENESIS	0.9268	1
HALLMARK_BILE_ACID_METABOLISM	0.9381	1
HALLMARK_PANCREAS_BETA_CELLS	0.9405	1
HALLMARK_ALLOGRAFT_REJECTION	0.9481	1
HALLMARK_HEME_METABOLISM	0.9549	1
HALLMARK_INTERFERON_GAMMA_RESPONSE	0.9629	1
HALLMARK_INFLAMMATORY_RESPONSE	0.9704	1
HALLMARK_ANGIOGENESIS	0.9902	1
HALLMARK_IL6_JAK_STAT3_SIGNALING	0.9955	1
HALLMARK_REACTIVE_OXIGEN_SPECIES_PATHWAY	0.9964	1
HALLMARK_ADIPOGENESIS	0.9986	1
HALLMARK_COMPLEMENT	0.9992	1
HALLMARK_P53_PATHWAY	0.9999	1
HALLMARK_XENOBIOTIC_METABOLISM	1	1
HALLMARK_COAGULATION	1	1
HALLMARK_IL2_STAT5_SIGNALING	1	1
HALLMARK_KRAS_SIGNALING_UP	1	1

Supplementary table 3 | Gene sets increased with age in encapsulated mskMPs compared to the young control after ten days *in-vivo*. GST Pval = Wilcoxon gene set test p-value. GST FDR = Adjusted p-value using the Benjamini-Hochberg procedure.

	Young								Aged				
Mouse	**1**	**2**	**3**	**4**	**5**	**6**	**7**	**8**	**1**	**2**	**3**	**4**	**5**
BLC	33.6	16.7	16.3	21.3	21.2	15.1	24.0	15.1	95.8	112.4	75.9	69.4	81.6
CD30L	35.2	3.1	13.2	6.7	15.2	6.9	21.8	18.8	37.9	14.3	19.5	0.4	3.1
Eotaxin	213.1	139.2	181.6	92.7	253.5	250.7	245.6	192.2	703.0	454.6	192.3	233.9	271.6
Eotaxin-2	125.8	66.0	71.5	72.6	57.8	52.9	153.6	78.4	329.8	174.2	75.9	49.2	22.6
Fas L	100.6	11.1	77.1	25.6	0.0	1.6	6.0	9.1	943.1	22.5	27.0	0.0	20.7
G-CSF	211.0	156.4	229.1	255.7	62.7	118.5	130.1	145.6	518.0	241.5	112.8	108.0	240.6
GM-CSF	16.1	12.6	12.0	16.2	27.0	19.2	27.2	25.3	35.6	34.6	16.2	11.6	24.5
ICAM-1	1765.7	1440.2	1896.0	1588.8	1871.7	1597.9	2409.4	1874.0	2260.4	5278.9	2393.3	2234.2	2339.1
IFNg	67.5	25.4	40.0	43.0	68.1	78.2	85.5	65.4	117.5	119.0	55.4	36.4	100.7
IL-1a	3.0	3.8	1.6	2.9	8.0	3.3	4.8	4.8	25.4	3.7	3.1	3.4	2.8
IL-1b	156.0	72.4	83.5	80.2	175.8	167.0	185.9	162.6	248.9	232.1	143.7	94.0	195.3
IL-2	88.0	74.8	84.9	69.0	123.7	114.0	121.2	97.2	170.0	118.8	74.5	91.7	99.1
IL-3	1.8	0.3	1.4	1.1	2.4	1.5	1.4	1.7	8.8	2.8	1.9	0.7	0.7
IL-4	3.6	0.8	1.7	1.9	1.5	1.1	0.8	1.3	12.1	2.2	2.9	0.4	2.4
IL-5	91.7	43.6	75.2	48.7	92.8	69.7	59.0	92.5	175.4	88.6	122.1	88.4	42.2
IL-6	11.9	3.0	17.9	9.7	17.0	14.7	14.6	15.9	43.3	19.2	10.9	11.4	28.9
IL-7	116.5	65.8	3.6	27.9	38.0	0.0	65.7	194.5	161.4	146.0	45.5	75.2	113.8
IL-10	287.5	139.5	147.3	142.0	340.5	292.4	316.5	323.1	311.4	358.1	194.9	207.9	299.1
IL-12p70	100.3	37.2	65.8	36.6	96.6	84.2	107.1	88.8	147.1	109.6	49.2	47.1	54.4
IL-13	31.4	0.0	0.9	6.4	0.0	0.0	3.1	0.0	198.2	59.5	21.9	0.0	0.0
IL-15	482.5	138.8	202.3	153.6	105.6	145.8	81.5	168.7	228.9	61.3	0.0	0.0	0.0
IL-17	3.6	1.7	2.7	0.9	2.0	1.2	3.6	1.8	14.8	2.2	3.8	2.0	9.2
IL-21	15.1	14.4	4.0	0.0	0.0	0.0	15.5	20.1	45.4	8.3	2.4	7.0	0.0
KC	3.7	2.9	2.9	2.7	3.9	3.5	3.9	3.2	4.6	4.8	3.5	2.8	3.7
Leptin	140.3	91.7	188.0	105.9	161.8	78.7	83.4	161.9	687.3	1930.5	220.0	325.6	84.3
LIX	356.0	322.0	292.9	230.1	531.1	381.0	482.4	392.8	512.4	663.4	18.0	257.4	411.3
MCP-1	45.0	20.3	21.4	16.8	37.7	32.9	45.0	40.9	69.6	17.1	18.5	17.7	20.2
MCP-5	53.2	25.8	19.8	11.6	40.9	20.9	11.1	31.4	67.1	15.3	41.5	12.7	11.6
MCSF	4.3	0.8	6.1	3.7	1.5	3.1	2.0	1.7	9.4	0.9	2.0	0.1	0.1
MIG	67.0	35.5	25.7	28.1	36.9	31.8	32.8	40.9	92.5	70.8	77.6	52.1	201.7
MIP-1a	8.4	10.3	19.6	8.9	12.8	12.6	10.8	12.5	32.5	26.3	17.7	15.1	2.0
PF4	3734.5	4274.5	4317.3	4222.6	3164.9	2978.8	3612.0	3644.5	3049.0	3336.7	4330.0	4125.5	2772.5
RANTES	1.7	1.3	2.2	1.4	2.1	1.8	1.5	1.8	5.7	5.2	3.1	2.5	0.1
TARC	35.2	14.0	19.5	12.1	30.0	20.1	36.6	20.7	44.1	34.6	21.4	13.3	16.0
TCA-3	34.7	23.5	23.3	10.4	45.4	14.2	38.8	30.2	40.2	34.9	63.9	18.7	25.9
TIMP-1	721.0	479.6	587.1	472.9	563.8	544.4	555.8	445.5	1055.8	851.2	830.4	505.2	694.6
TNFa	28.0	19.2	18.2	22.7	44.8	34.4	42.6	44.5	64.1	50.0	29.7	23.1	35.7
TNF RII	416.2	209.0	373.4	259.0	396.6	367.6	306.4	113.3	439.8	542.5	401.2	225.7	248.6

Supplementary table 4 | Multiplexed ELISA array quantification of levels of inflammatory factors in plasma of mice young and aged mice. n≥5 mice. Each value represents averages in pg/ml from n=4 technical replicates for each factor. TNF-RI and MIP-1g were excluded from the analysis since signals were outside of the detection range.

Gene Set Name - Human	GST Pval	GST FDR
HALLMARK_TNFA_SIGNALING_VIA_NFKB	1.00E-04	0.0025
HALLMARK_MYOGENESIS	1.00E-04	0.0025
HALLMARK_ESTROGEN_RESPONSE_EARLY	4.00E-04	0.006666667
HALLMARK_INFLAMMATORY_RESPONSE	0.0012	0.015
HALLMARK_KRAS_SIGNALING_DN	0.0022	0.018571429
HALLMARK_HYPOXIA	0.0026	0.018571429
HALLMARK_INTERFERON_GAMMA_RESPONSE	0.0026	0.018571429
HALLMARK_PI3K_AKT_MTOR_SIGNALING	0.004	0.025
HALLMARK_IL6_JAK_STAT3_SIGNALING	0.0067	0.037222222
HALLMARK_MITOTIC_SPINDLE	0.0082	0.041
HALLMARK_P53_PATHWAY	0.0112	0.04875
HALLMARK_NOTCH_SIGNALING	0.0117	0.04875
HALLMARK_APICAL_JUNCTION	0.0139	0.053461538
HALLMARK_INTERFERON_ALPHA_RESPONSE	0.0159	0.055
HALLMARK_UNFOLDED_PROTEIN_RESPONSE	0.0165	0.055
HALLMARK_EPITHELIAL_MESENCHYMAL_TRANSITION	0.022	0.06875
HALLMARK_APOPTOSIS	0.0246	0.072352941
HALLMARK_UV_RESPONSE_DN	0.0331	0.085714286
HALLMARK_IL2_STAT5_SIGNALING	0.0352	0.085714286
HALLMARK_COMPLEMENT	0.0353	0.085714286
HALLMARK_GLYCOLYSIS	0.036	0.085714286
HALLMARK_ESTROGEN_RESPONSE_LATE	0.0493	0.112045455
HALLMARK_HEDGEHOG_SIGNALING	0.0537	0.11673913
HALLMARK_APICAL_SURFACE	0.0593	0.123541667
HALLMARK_UV_RESPONSE_UP	0.0726	0.1452
HALLMARK_MTORC1_SIGNALING	0.0827	0.159038462
HALLMARK_ALLOGRAFT_REJECTION	0.2044	0.378518519
HALLMARK_DNA_REPAIR	0.225	0.401785714
HALLMARK_HEME_METABOLISM	0.2687	0.449193548
HALLMARK_PEROXISOME	0.2711	0.449193548
HALLMARK_TGF_BETA_SIGNALING	0.2785	0.449193548
HALLMARK_BILE_ACID_METABOLISM	0.3176	0.49625
HALLMARK_MYC_TARGETS_V2	0.376	0.56969697
HALLMARK_CHOLESTEROL_HOMEOSTASIS	0.4723	0.694558824
HALLMARK_PROTEIN_SECRETION	0.5884	0.840571429
HALLMARK_ANDROGEN_RESPONSE	0.6312	0.857837838
HALLMARK_WNT_BETA_CATENIN_SIGNALING	0.6348	0.857837838
HALLMARK_SPERMATOGENESIS	0.6707	0.8825
HALLMARK_REACTIVE_OXIGEN_SPECIES_PATHWAY	0.7166	0.896875
HALLMARK_G2M_CHECKPOINT	0.7175	0.896875
HALLMARK_ADIPOGENESIS	0.7542	0.919756098
HALLMARK_XENOBIOTIC_METABOLISM	0.8072	0.952790698
HALLMARK_KRAS_SIGNALING_UP	0.8194	0.952790698
HALLMARK_COAGULATION	0.9334	1
HALLMARK_ANGIOGENESIS	0.9352	1
HALLMARK_PANCREAS_BETA_CELLS	0.9707	1
HALLMARK_FATTY_ACID_METABOLISM	0.9777	1
HALLMARK_E2F_TARGETS	0.9846	1
HALLMARK_OXIDATIVE_PHOSPHORYLATION	0.9996	1
HALLMARK_MYC_TARGETS_V1	1	1

Supplementary table 5 | Gene sets decreased with age in encapsulated hskMPs compared to the young control after ten days *in-vivo*. GST Pval = Wilcoxon gene set test p-value. GST FDR = Adjusted p-value using the Benjamini-Hochberg procedure.

Gene Set Name - Mouse	GST Pval	GST FDR
HALLMARK_XENOBIOTIC_METABOLISM	1.00E-04	0.001
HALLMARK_P53_PATHWAY	1.00E-04	0.001
HALLMARK_COAGULATION	1.00E-04	0.001
HALLMARK_IL2_STAT5_SIGNALING	1.00E-04	0.001
HALLMARK_KRAS_SIGNALING_UP	1.00E-04	0.001
HALLMARK_COMPLEMENT	8.00E-04	0.006666667
HALLMARK_ADIPOGENESIS	0.0018	0.012857143
HALLMARK_IL6_JAK_STAT3_SIGNALING	0.0036	0.0225
HALLMARK_REACTIVE_OXIGEN_SPECIES_PATHWAY	0.0043	0.023888889
HALLMARK_ANGIOGENESIS	0.0089	0.0445
HALLMARK_INFLAMMATORY_RESPONSE	0.0296	0.134545455
HALLMARK_INTERFERON_GAMMA_RESPONSE	0.0348	0.145
HALLMARK_HEME_METABOLISM	0.0391	0.150384615
HALLMARK_ALLOGRAFT_REJECTION	0.0561	0.198823529
HALLMARK_PANCREAS_BETA_CELLS	0.0606	0.198823529
HALLMARK_BILE_ACID_METABOLISM	0.0648	0.198823529
HALLMARK_MYOGENESIS	0.0676	0.198823529
HALLMARK_PROTEIN_SECRETION	0.0918	0.255
HALLMARK_EPITHELIAL_MESENCHYMAL_TRANSITION	0.1071	0.268809524
HALLMARK_ESTROGEN_RESPONSE_EARLY	0.1125	0.268809524
HALLMARK_GLYCOLYSIS	0.1129	0.268809524
HALLMARK_UV_RESPONSE_UP	0.1237	0.281136364
HALLMARK_DNA_REPAIR	0.1388	0.30173913
HALLMARK_WNT_BETA_CATENIN_SIGNALING	0.1468	0.305833333
HALLMARK_HYPOXIA	0.1736	0.334038462
HALLMARK_PEROXISOME	0.1737	0.334038462
HALLMARK_APOPTOSIS	0.183	0.33625
HALLMARK_UNFOLDED_PROTEIN_RESPONSE	0.1883	0.33625
HALLMARK_INTERFERON_ALPHA_RESPONSE	0.2077	0.3485
HALLMARK_APICAL_SURFACE	0.2091	0.3485
HALLMARK_TNFA_SIGNALING_VIA_NFKB	0.2938	0.473870968
HALLMARK_SPERMATOGENESIS	0.3287	0.51359375
HALLMARK_ESTROGEN_RESPONSE_LATE	0.3518	0.533030303
HALLMARK_MTORC1_SIGNALING	0.3919	0.576323529
HALLMARK_FATTY_ACID_METABOLISM	0.4534	0.640555556
HALLMARK_OXIDATIVE_PHOSPHORYLATION	0.4612	0.640555556
HALLMARK_ANDROGEN_RESPONSE	0.5669	0.766081081
HALLMARK_PI3K_AKT_MTOR_SIGNALING	0.5979	0.768333333
HALLMARK_APICAL_JUNCTION	0.5993	0.768333333
HALLMARK_TGF_BETA_SIGNALING	0.7692	0.9615
HALLMARK_NOTCH_SIGNALING	0.8402	1
HALLMARK_CHOLESTEROL_HOMEOSTASIS	0.873	1
HALLMARK_KRAS_SIGNALING_DN	0.8786	1
HALLMARK_HEDGEHOG_SIGNALING	0.9466	1
HALLMARK_UV_RESPONSE_DN	0.9712	1
HALLMARK_MYC_TARGETS_V2	0.9741	1
HALLMARK_MITOTIC_SPINDLE	1	1
HALLMARK_G2M_CHECKPOINT	1	1
HALLMARK_E2F_TARGETS	1	1
HALLMARK_MYC_TARGETS_V1	1	1

Supplementary table 6 | Gene sets decreased with age in encapsulated mskMPs compared to the young control after ten days *in-vivo*. GST Pval = Wilcoxon gene set test p-value. GST FDR = Adjusted p-value using the Benjamini-Hochberg procedure.

Gene Set Name - Freshly Isolated MPs	GST Pval	GST FDR
HALLMARK_TNFA_SIGNALING_VIA_NFKB	1.00E-04	0.000714286
HALLMARK_INTERFERON_ALPHA_RESPONSE	1.00E-04	0.000714286
HALLMARK_INTERFERON_GAMMA_RESPONSE	1.00E-04	0.000714286
HALLMARK_E2F_TARGETS	1.00E-04	0.000714286
HALLMARK_XENOBIOTIC_METABOLISM	1.00E-04	0.000714286
HALLMARK_FATTY_ACID_METABOLISM	1.00E-04	0.000714286
HALLMARK_ALLOGRAFT_REJECTION	1.00E-04	0.000714286
HALLMARK_MTORC1_SIGNALING	2.00E-04	0.001111111
HALLMARK_MYC_TARGETS_V2	2.00E-04	0.001111111
HALLMARK_OXIDATIVE_PHOSPHORYLATION	4.00E-04	0.002
HALLMARK_G2M_CHECKPOINT	8.00E-04	0.003636364
HALLMARK_IL6_JAK_STAT3_SIGNALING	0.0028	0.011153846
HALLMARK_INFLAMMATORY_RESPONSE	0.0029	0.011153846
HALLMARK_REACTIVE_OXIGEN_SPECIES_PATHWAY	0.0039	0.013928571
HALLMARK_MYC_TARGETS_V1	0.0047	0.015666667
HALLMARK_APOPTOSIS	0.0074	0.023125
HALLMARK_BILE_ACID_METABOLISM	0.0194	0.057058824
HALLMARK_KRAS_SIGNALING_UP	0.0265	0.073611111
HALLMARK_COMPLEMENT	0.0371	0.097631579
HALLMARK_DNA_REPAIR	0.0452	0.113
HALLMARK_PEROXISOME	0.0858	0.204285714
HALLMARK_SPERMATOGENESIS	0.1062	0.241363636
HALLMARK_GLYCOLYSIS	0.1574	0.342173913
HALLMARK_APICAL_SURFACE	0.2034	0.42375
HALLMARK_ESTROGEN_RESPONSE_LATE	0.2152	0.4304
HALLMARK_IL2_STAT5_SIGNALING	0.2275	0.4375
HALLMARK_ADIPOGENESIS	0.2721	0.503888889
HALLMARK_CHOLESTEROL_HOMEOSTASIS	0.2845	0.508035714
HALLMARK_UNFOLDED_PROTEIN_RESPONSE	0.326	0.562068966
HALLMARK_PANCREAS_BETA_CELLS	0.39	0.65
HALLMARK_HEME_METABOLISM	0.4151	0.65890625
HALLMARK_COAGULATION	0.4217	0.65890625
HALLMARK_P53_PATHWAY	0.4672	0.707878788
HALLMARK_HYPOXIA	0.4937	0.726029412
HALLMARK_ANDROGEN_RESPONSE	0.556	0.794285714
HALLMARK_PI3K_AKT_MTOR_SIGNALING	0.5926	0.823055556
HALLMARK_UV_RESPONSE_UP	0.7824	1
HALLMARK_ESTROGEN_RESPONSE_EARLY	0.8029	1
HALLMARK_WNT_BETA_CATENIN_SIGNALING	0.8277	1
HALLMARK_PROTEIN_SECRETION	0.841	1
HALLMARK_TGF_BETA_SIGNALING	0.9167	1
HALLMARK_NOTCH_SIGNALING	0.9188	1
HALLMARK_HEDGEHOG_SIGNALING	0.9471	1
HALLMARK_MITOTIC_SPINDLE	0.9955	1
HALLMARK_KRAS_SIGNALING_DN	0.9984	1
HALLMARK_MYOGENESIS	0.9994	1
HALLMARK_APICAL_JUNCTION	0.9996	1
HALLMARK_UV_RESPONSE_DN	0.9999	1
HALLMARK_EPITHELIAL_MESENCHYMAL_TRANSITION	1	1
HALLMARK_ANGIOGENESIS	1	1

Supplementary table 7 | Gene sets increased with age in niche resident freshly isolated mouse muscle stem cells compared to the young control. GST Pval = Wilcoxon gene set test p-value. GST FDR = Adjusted p-value using the Benjamini-Hochberg procedure.

Gene Set Name - Freshly Isolated MPs	GST Pval	GST FDR
HALLMARK_EPITHELIAL_MESENCHYMAL_TRANSITION	1.00E-04	0.001666667
HALLMARK_UV_RESPONSE_DN	1.00E-04	0.001666667
HALLMARK_ANGIOGENESIS	1.00E-04	0.001666667
HALLMARK_MYOGENESIS	2.00E-04	0.0025
HALLMARK_APICAL_JUNCTION	4.00E-04	0.004
HALLMARK_KRAS_SIGNALING_DN	0.0019	0.015833333
HALLMARK_MITOTIC_SPINDLE	0.0055	0.039285714
HALLMARK_HEDGEHOG_SIGNALING	0.0509	0.318125
HALLMARK_NOTCH_SIGNALING	0.0785	0.435
HALLMARK_TGF_BETA_SIGNALING	0.087	0.435
HALLMARK_PROTEIN_SECRETION	0.1603	0.728636364
HALLMARK_WNT_BETA_CATENIN_SIGNALING	0.1808	0.739615385
HALLMARK_ESTROGEN_RESPONSE_EARLY	0.1923	0.739615385
HALLMARK_UV_RESPONSE_UP	0.2166	0.773571429
HALLMARK_PI3K_AKT_MTOR_SIGNALING	0.3975	1
HALLMARK_ANDROGEN_RESPONSE	0.4511	1
HALLMARK_HYPOXIA	0.5136	1
HALLMARK_P53_PATHWAY	0.5311	1
HALLMARK_COAGULATION	0.585	1
HALLMARK_HEME_METABOLISM	0.5856	1
HALLMARK_PANCREAS_BETA_CELLS	0.6043	1
HALLMARK_UNFOLDED_PROTEIN_RESPONSE	0.667	1
HALLMARK_CHOLESTEROL_HOMEOSTASIS	0.7074	1
HALLMARK_ADIPOGENESIS	0.7445	1
HALLMARK_IL2_STAT5_SIGNALING	0.768	1
HALLMARK_ESTROGEN_RESPONSE_LATE	0.7814	1
HALLMARK_APICAL_SURFACE	0.8004	1
HALLMARK_GLYCOLYSIS	0.8457	1
HALLMARK_SPERMATOGENESIS	0.8918	1
HALLMARK_PEROXISOME	0.9184	1
HALLMARK_DNA_REPAIR	0.9581	1
HALLMARK_COMPLEMENT	0.9625	1
HALLMARK_KRAS_SIGNALING_UP	0.9756	1
HALLMARK_BILE_ACID_METABOLISM	0.9823	1
HALLMARK_APOPTOSIS	0.9911	1
HALLMARK_REACTIVE_OXIGEN_SPECIES_PATHWAY	0.9948	1
HALLMARK_MYC_TARGETS_V1	0.9957	1
HALLMARK_IL6_JAK_STAT3_SIGNALING	0.9977	1
HALLMARK_INFLAMMATORY_RESPONSE	0.9982	1
HALLMARK_MTORC1_SIGNALING	0.9998	1
HALLMARK_G2M_CHECKPOINT	0.9999	1
HALLMARK_FATTY_ACID_METABOLISM	0.9999	1
HALLMARK_TNFA_SIGNALING_VIA_NFKB	1	1
HALLMARK_INTERFERON_ALPHA_RESPONSE	1	1
HALLMARK_INTERFERON_GAMMA_RESPONSE	1	1
HALLMARK_E2F_TARGETS	1	1
HALLMARK_MYC_TARGETS_V2	1	1
HALLMARK_XENOBIOTIC_METABOLISM	1	1
HALLMARK_OXIDATIVE_PHOSPHORYLATION	1	1
HALLMARK_ALLOGRAFT_REJECTION	1	1

Supplementary table 8 | Gene sets decreased with age in niche resident freshly isolated mouse muscle stem cells compared to the young control. GST Pval = Wilcoxon gene set test p-value. GST FDR = Adjusted p-value using the Benjamini-Hochberg procedure.

Upregulated			
GO-Term - Mouse	**GST Pval**	**GST FDR**	**Cluster**
GO_RNA_SPLICING_VIA_TRANSESTERIFICATION_REACTIONS	1.00E-04	0.003475882	Related to gene expression cluster **II**
GO_REGULATION_OF_MRNA_SPLICING_VIA_SPLICEOSOME	0.0012	0.024967606	Related to gene expression cluster **II**
GO_REGULATION_OF_NEURON_DIFFERENTIATION	0.0081	0.099095031	Related to gene expression cluster **V**
GO_RNA_PROCESSING	1.00E-04	0.003475882	Related to gene expression cluster **IX**
GO_PANCREAS_DEVELOPMENT	0.0177	0.172021875	Related to gene expression cluster **X**

Downregulated			
GO-Term - Mouse	**GST Pval**	**GST FDR**	**Cluster**
GO_RESPONSE_TO_INTERFERON_BETA	0.0113	0.181939237	Related to gene expression cluster **VI**
GO_POSITIVE_REGULATION_OF_TYROSINE_PHOSPHORYLATION_OF_STAT5_PROTEIN	0.0709	0.443800953	Related to gene expression cluster **VII**
GO_POSITIVE_REGULATION_OF_PEPTIDYL_TYROSINE_PHOSPHORYLATION	0.0715	0.44519863	Related to gene expression cluster **VII**
GO_DEFENSE_RESPONSE_TO_OTHER_ORGANISM	0.0028	0.081906931	Related to gene expression cluster **VIII**

Supplementary table 9 | Gene ontology (GO) terms perturbed in encapsulated mskMPs in the young and aged condition overlapping with those affected in choroid plexus tissue of heterochronic relative to isochronic mouse parabionts (Baruch et al. Science, 2014). Baruch et al. generated gene expression clusters based on K-means using Squared Euclidean distance as the correlation metrics and determined GO terms significantly enriched in each individual cluster. Cluster II contains GO terms for RNA splicing. Cluster V contains GO terms for ion homeostasis, neuron differentiation, morphogenesis, and endothelial cell migration. Cluster VI contains GO terms for interferon related processes and response to virus. Cluster VII contains GO terms for tyrosine phosphorylation and JAK-STAT signaling. Cluster VIII contains GO terms for immune response, peptidase activity, response to other organism. Cluster IX contains GO terms for metabolic processes and RNA processing. Cluster X contains GO terms for pancreas development and microtubule regulation. GST Pval = Wilcoxon gene set test p-value. GST FDR = Adjusted p-value using the Benjamini-Hochberg procedure.

Upregulated			
GO-Term - Human	**GST Pval**	**GST FDR**	**Cluster**
GO_NCRNA_PROCESSING	0.0011	0.088406849	Related to gene expression cluster **IX**
GO_RNA_PROCESSING	0.0018	0.11734	Related to gene expression cluster **IX**

Downregulated			
GO-Term - Human	**GST Pval**	**GST FDR**	**Cluster**
GO_LEUKOCYTE_MIGRATION	0.0012	0.046625166	Related to gene expression cluster **III**
GO_CELL_MOTILITY	0.0072	0.119666856	Related to gene expression cluster **III**
GO_REGULATION_OF_CELL_ADHESION	0.0111	0.150711927	Related to gene expression cluster **III**
GO_VASCULAR_ENDOTHELIAL_GROWTH_FACTOR_SIGNALING_PATHWAY	0.0049	0.098791409	Related to gene expression cluster **IV**
GO_ANGIOGENESIS	0.0259	0.227477994	Related to gene expression cluster **IV**
GO_REGULATION_OF_NEURON_DIFFERENTIATION	1.00E-04	0.013644186	Related to gene expression cluster **V**
GO_REGULATION_OF_ANATOMICAL_STRUCTURE_MORPHOGENESIS	0.0058	0.108717572	Related to gene expression cluster **V**
GO_RESPONSE_TO_TYPE_I_INTERFERON	3.00E-04	0.021464634	Related to gene expression cluster **VI**
GO_RESPONSE_TO_VIRUS	0.0026	0.070621296	Related to gene expression cluster **VI**
GO_RESPONSE_TO_INTERFERON_BETA	0.0182	0.193091139	Related to gene expression cluster **VI**
GO_IMMUNE_RESPONSE	1.00E-04	0.013644186	Related to gene expression cluster **VIII**
GO_INNATE_IMMUNE_RESPONSE	4.00E-04	0.025508696	Related to gene expression cluster **VIII**

Supplementary table 10 | Gene ontology (GO) terms perturbed in encapsulated hskMPs in the young and aged condition overlapping with those affected in choroid plexus tissue of heterochronic relative to isochronic mouse parabionts (Baruch et al. Science, 2014). Baruch et al. generated gene expression clusters based on K-means using Squared Euclidean distance as the correlation metrics and determined GO terms significantly enriched in each individual cluster. Cluster III contains GO terms for cell motility, migration, adhesion, and metal ion homeostasis. Cluster IV contains GO terms for fibril organization, angiogenesis, morphogenesis, VEGF signaling. Cluster V contains GO terms for ion homeostasis, neuron differentiation, morphogenesis, and endothelial cell migration. Cluster VI contains GO terms for interferon related processes and response to virus. Cluster VIII contains GO terms for immune response, peptidase activity, response to other organism. Cluster IX contains GO terms for metabolic processes and RNA processing. GST Pval = Wilcoxon gene set test p-value. GST FDR = Adjusted p-value using the Benjamini-Hochberg procedure.